NASA TN D-1557

TECHNICAL NOTE
D-1557

AERODYNAMIC CHARACTERISTICS IN GROUND EFFECT OF A LARGE-SCALE MODEL WITH A HIGH DISK-LOADING LIFTING FAN MOUNTED IN THE FUSELAGE

By Richard A. deSavigny and David H. Hickey

Ames Research Center
Moffett Field, Calif.

NATIONAL AERONAUTICS AND SPACE ADMINISTRATION
WASHINGTON
January 1963

NATIONAL AERONAUTICS AND SPACE ADMINISTRATION

TECHNICAL NOTE D-1557

AERODYNAMIC CHARACTERISTICS IN GROUND EFFECT OF A LARGE-SCALE MODEL WITH A HIGH DISK-LOADING LIFTING FAN MOUNTED IN THE FUSELAGE

By Richard A. deSavigny and David H. Hickey

SUMMARY

An investigation was conducted to determine the longitudinal characteristics in ground effect of a large-scale VTOL airplane model with a direct lifting fan enclosed in the fuselage. The model had a shoulder-mounted unswept wing of aspect ratio 5. Characteristics of the model with and without the horizontal tail were obtained with the wing at 1.83 and 2.39 fan diameters from the simulated ground plane installed above the wind-tunnel floor. Test airspeeds ranged from 20 to 80 knots. A trailing-edge flap deflected 30° was used throughout the investigation.

Static performance in ground effect, three-component longitudinal characteristics, static-pressure distributions on the fuselage and downwash at the horizontal tail are included herein.

INTRODUCTION

Reference 1 reports an investigation of the aerodynamic characteristics of a large-scale model with a high disk-loading fan mounted in the fuselage. The present investigation was conducted to obtain aerodynamic characteristics of the same model in ground effect for evaluation of STOL and VTOL performance. Other studies conducted on this model are reported in references 2, 3, 4, and 5.

For this investigation a ground plane was installed and the model was mounted on the Ames 40- by 80-Foot Wind Tunnel variable-height strut system. The model was tested with and without the horizontal tail through the STOL and VTOL airspeed-power spectrum. Trailing-edge flaps were deflected 30° throughout the investigation.

General aerodynamic characteristics of the model and some fan performance and fuselage pressure distribution data were measured. The results are presented with only a brief analysis in order to expedite publication.

NOTATION

A	fan exit area, sq ft
a	vertical distance from the top of the fuselage at the fan to a point on the inlet bellmouth, in.
b	wing span, ft
c	wing chord parallel to plane of symmetry, ft
$\bar{c}$	mean aerodynamic chord, $\frac{2}{S}\int_0^{b/2} c^2 dy$
C_L	lift coefficient, $\frac{L}{q_\infty S}$
C_D	drag coefficient, $\frac{D}{q_\infty S}$
C_m	pitching-moment coefficient, $\frac{M}{q_\infty S \bar{c}}$
D	drag, lb
d	fan diameter, ft
h	vertical distance from the wing chord plane to the ground plane, ft
i_t	horizontal-tail incidence angle, deg
L	total lift on model, lb
M	pitching moment about the moment center shown in figure 2, ft-lb
p	pressure coefficient, $\frac{p_l - p_s}{q_\infty}$
p_l	local static pressure, lb/sq ft
p_s	test section static pressure, lb/sq ft
p_o	pressure at standard atmosphere, 2116 lb/sq ft
q	dynamic pressure, lb/sq ft
R	Reynolds number (or fan radius, ft)
RPM	correct fan rotation speed
r	distance from fan rotation axis, ft

S wing area, sq ft

T complete ducted fan thrust in the lift direction, $\rho A v_j^2$, lb

V air velocity, knots

v air velocity, ft/sec

x distance from leading edge to some point on the airfoil or flaps, ft

y spanwise distance perpendicular to the plane of symmetry, ft

Z vertical distance from the bottom of the fuselage at the fan to the ground plane, ft

z perpendicular distance from the chord line to the airfoil surface, ft

α angle of attack of fuselage reference line, deg

β fan exit vane deflection measured normal to the pivot line and from the fan axis, deg

δ relative static pressure, $\frac{p_s}{p_o}$

δ_f trailing-edge flap deflection measured normal to the hinge line, deg

ϵ average downwash angle at the horizontal tail, deg

η fraction of wing semispan, $\frac{2y}{b}$

ρ density of air, slugs/cu ft

μ tip-speed ratio, $\frac{V_\infty}{\omega R}$

ω rotational speed, radians/sec

Subscripts

j fan exit

s static conditions

∞ free stream

MODEL AND APPARATUS

Figure 1 is photographs of the model mounted on the variable-height strut system in the Ames 40- by 80-Foot Wind Tunnel. The ground plane is also shown. A sketch of the model giving pertinent dimensions is shown in figure 2.

Wing Geometry

The wing had an aspect ratio of 5.0, taper ratio of 0.5, and sweepback of 0° at the quarter-chord line. The wing employed NACA 63A-210 airfoil sections parallel to the fuselage line of symmetry. The upper surface of the wing was tangent with the top of the fuselage. Coordinates of the wing sections are listed in table I.

Details of the single-slotted trailing-edge flap are shown in figure 3, and flap ordinates are given in table II. The flap tested extended from 0.21 to 0.60 semispan and was deflected 30° throughout the test.

Fuselage

Figure 4 is a sketch of the fuselage showing the cross sections and static-pressure orifices. Further details of the fuselage are given in reference 1.

Lifting-Fan Unit

The General Electric X-353-5 lifting-fan engine consists of a fan driven by exhaust gases from a gas generator. The exhaust gases from the J85-7 generator are channeled through a turbine at the tip of the fan.

Fan details.- To provide good flow into the fan, the fan was mounted near the bottom of the fuselage with a long duct extending to the inlet on top of the fuselage. Details of the fan installation are shown in figure 5. An airfoil cascade to vector the fan thrust was mounted immediately under the fan. The fan axis intersected the quarter-chord line of the wing and was perpendicular to the wing chord plane. A suspension framework supported the J-85 gas generator below and to the right of the fuselage. Details of the gas generator installation and location are shown in figures 1 and 2.

The single-stage fan rotor had 36 blades and a 62.5-inch fan diameter. A single stage of stators was employed behind the rotor. Exit vanes were mounted downstream of the stators. These vanes could be deflected from -15° to $+75^\circ$ (full duct closure). The span of the vanes extended across the tip turbine exhaust. The vane airfoil section had a maximum thickness of 10-percent chord at 20-percent chord and had a maximum of 2.3-percent chord camber of the mean

line at 35-percent chord. Mechanical wear in the exit vane suspension system made it difficult to maintain exit vane deflections accurately during this investigation.

Fan inlet.- Photographs and sketches of the inlet are shown in figure 5. The front half of the inlet (coordinates in table III) had a varying radius from 0.23 to 0.06 of the fan diameter; the rear half had a constant radius of 0.06 of the fan diameter. A semicircular inlet vane with a 22.71-inch chord was mounted in the front portion of the inlet. The inlet vane airfoil section was made up of a 6-inch wedge attached to the trailing edge of a conventional airfoil section. The upper side of the wedge was tangent to the upper surface of the airfoil trailing edge and the lower side was faired into the bottom of the airfoil. The resultant airfoil section was 10 percent chord thick with 10.5-percent-chord camber of the mean line.

TESTING AND PROCEDURE

Force and moment data were obtained through an angle-of-attack range from -4° to $+16^\circ$. A flap extending from 0.21 to 0.60 semispan was deflected 30° throughout the investigation. Some fan performance data and pressure distributions on the fuselage were obtained.

As in reference 1, aerodynamic force and moment coefficients will be presented as functions of tip speed ratio. For convenience in testing, full-scale tip speed ratios were duplicated by reducing fan rpm and lowering wind-tunnel dynamic pressure. The airspeed of the tests varied from 20 to 80 knots; the top test speed corresponds to the tip speed ratio for 125 knots at full power. Maximum Reynolds number was 6.3 million. Fan rpm was varied from 1100 to 2450 rpm.

Angle of attack was held constant at 0° while fan rpm and wind-tunnel velocity were varied. Results were obtained with several exit-vane deflections and with the horizontal tail on and off.

Fan rpm was maintained essentially constant while angle of attack was varied. The model variables tested in this manner are mentioned above.

CORRECTIONS

No wind-tunnel boundary corrections were applied to the force data. Corrections to dynamic pressure due to blockage of the wind-tunnel test section by the ground plane and large variable-height struts have been included in the results. Lift, drag, and moment have been corrected for the effects of the variable-height struts. Comparable corrections were made to the data in reference 1 presented herein.

It should be realized that the air flowing through the unconventionally positioned gas generator makes small contributions to lift, drag, and moment. The test results include these forces and moments.

During the investigation the exit vanes were continuously loosening, introducting the possibility of small discrepancies in exit-vane angle readings. Since the discrepancies were not consistent, exit-vane angle corrections could not be applied.

Reingestion of exhaust gases from the fan turbine at zero airspeed made it necessary to obtain static lift data at approximately 20 knots airspeed. Lift data were corrected to zero airspeed by subtracting the lift at 20 knots with the power off. Drag results were corrected for ram drag.

RESULTS

Tests were conducted at two ground heights, $h/d = 1.83$ and 2.39. The results from reference 1, included on some of the figures for comparison, are considered to be for $h/d = 3.96$.

Zero Airspeed Characteristics

Lift and drag results corrected to zero airspeed are presented in figures 6 through 8. Figure 6 shows the variation of static lift with fan rpm for the three ground heights (including that of ref. 1) and three exit louver deflections. The variation of static lift with thrust (negative drag) for fixed exit-vane angles is presented in figure 7 for the two ground plane heights. Data from reference 1 are included in the figures.

Figure 8 shows the ratio of the static lift at various ground heights to the lift at $h/d = 3.96$ as a function of h/d. Included on this figure is the fan thrust determined from measured values of fan airflow.

Aerodynamic Characteristics

0° angle of attack.- Figures 9 through 16 show the effect of fan speed and airspeed (tip-speed ratio) on various aerodynamic characteristics at 0° angle of attack. The ratio of lift at forward speed to lift at zero airspeed is shown as a function of tip-speed ratio in figure 9 at 0° exit-vane angle for all ground plane heights. Figures 9(a) and (b) differ only in the values of lift at zero airspeed: in figure 9(a) the value was measured in ground effect while in figure 9(b) it was measured at $h/d = 3.96$. Figures 10 and 11 show the variation of lift, drag, and pitching-moment coefficients with tip-speed ratio at the ground heights under consideration for several exit-vane angles. Data in figure 10

represent characteristics with the horizontal tail removed and in figure 11 with the tail on, and both figures include comparable data from reference 1.

Figures 12 through 15 show pressure distributions on the top and bottom of the fuselage at the two ground heights, four tip-speed ratios, and several exit-vane angles. (See fig. 4 for pressure orifice locations.) Pressure distributions corresponding to $h/d = 3.96$ are shown in figure 17 of reference 1. Figure 16 shows the change in average downwash at the horizontal tail due to fan operation with 0° exit-vane angle. The two ground heights and the one presented in reference 1 are represented. These results were computed from the data in figures 10 and 11 and the tail effectiveness presented in reference 1.

Variable angle-of-attack results.- Figures 17 and 18 show longitudinal characterisitcs with the fan power off. Data in figure 17 show the effect of ground height on longitudinal characteristics, including results from reference 1.

Figures 19 through 27 present longitudinal characteristics in coefficient form with the lifting-fan operating. Data in figures 19 through 21 were obtained with the horizontal tail off. Results shown in figure 19 are with 0° exit-vane angle at several tip speed ratios for both ground heights. Similar results for 20° and 35° exit-vane angles are shown in figure 20 and 21, respectively.

Figures 22 through 27 present longitudinal characteristics with the horizontal tail on. The results shown in figure 22 are for 0° exit-vane angle, 20 knots, and both ground heights. Figure 23 presents results at 30 knots airspeed with exit-vane angles of 0° and 35° for both ground heights. Figures 24 and 25 present results at 40 and 60 knots, respectively, with exit-vane angles of 0°, 20°, and 35° for three ground heights.

Longitudinal characteristics presented in figure 26, representing 0° exit-vane angle and near constant tip-speed ratio, were obtained at 60 and 80 knots airspeed. Figure 27 presents results obtained at 60 knots for three exit-vane angles at the low ground height.

Discussion of Adverse Ground Effect

Results in figure 8 show that ground proximity reduced total static lift 13 percent at $h/d = 2.39$ and 33 percent at $h/d = 1.83$.

Pressure instrumentation at the fan efflux was inadequate for measuring fan thrust directly; however, fan airflow could be measured with pressure instrumentation in the fan inlet. Figure 37 of reference 5 shows the variation of thrust with fan airflow reduction. These results in conjunction with the measured airflow in ground effect were used to compute the fan thrust in ground effect shown in figure 8. This is an estimated curve since an extrapolation to zero velocity had to be used to obtain static fan airflow. Figure 8 shows that approximately 60 percent of the lift loss in ground effect was due to fan thrust reduction.

Total pressure profiles at the fan exit indicated this thrust loss was due to fan stall in the region of the hub. It is probable that the stall was influenced by the low pressure at the hub radius because of the long inlet duct and the high pressure area at the base of the fan hub resulting from ground proximity. This supposition is supported by recent static tests in ground effect with fan-in-the-wing installation having a short inlet, which indicated a much smaller ground effect on fan thrust. Therefore, it is probable that the adverse ground effect on fan stall is a function of fan inlet flow profile as well as back pressure on the fan. The remaining 40 percent of the lift loss is attributed to fan-induced flow effects on the model. Pressure measurements on the bottom of the fuselage indicate that at low airspeeds as height above the ground plane is reduced there is an increase in negative pressure that would result in a significant lift loss.

In general, two variables altered the amount of lift loss in ground effect: forward speed and exit-vane deflection. As seen in figure 9, the effect of forward speed on lift at 0° exit-vane angle was to reduce the lift loss to zero at $\mu = 0.252$ (approximately 107 knots at 2600 rpm). Results in figures 23 through 25 show the effect of exit-vane deflection on lift was to reduce the lift loss caused by ground proximity. Out of ground effect, an increase in exit-vane angle will reduce lift while increasing horizontal force. Results in figure 25 show that at $\mu = 0.23$ (approximately 93 knots at 2600 rpm), practically all the lift reduction due to changing lift to thrust by deflecting exit vanes was regained. At 35° exit-vane angle, there is an actual net lift increase in ground effect.

Ames Research Center
National Aeronautics and Space Administration
Moffett Field, Calif., Sept. 28, 1962

REFERENCES

1. Aoyagi, Kiyoshi, Hickey, David H., and deSavigny, Richard A.: Aerodynamic Characteristics of a Large-Scale Model With a High Disk-Loading Lifting Fan Mounted in the Fuselage. NASA TN D-775, 1961.

2. Maki, Ralph L., and Hickey David H.: Aerodynamics of a Fan-in-Fuselage Model. NASA TN D-789, 1961.

3. Anon.: Results of Wind-Tunnel Tests of a Full-Scale Fuselage-Mounted, Tip-Turbine-Driven Lift Fan. U.S. Army TRECOM TR 61-15, vol. 1, Jan. 1961.

4. Anon.: Results of Wind-Tunnel Tests of a Full-Scale Fuselage-Mounted, Tip-Turbine-Driven Lift Fan. U.S. Army TRECOM TR 61-15, vol. 2, Jan. 1961.

5. Przedpelski, Z. J.: Results of Wind-Tunnel Tests of a Full-Scale Fuselage-Mounted, Tip-Turbine-Driven Lift Fan. U.S. Army TRECOM TR 61-15, vol. 3, Jan. 1961.

TABLE I.- COORDINATES OF WING AIRFOIL SECTION (NACA 63A-210) PARALLEL TO THE MODEL PLANE OF SYMMETRY

Upper surface		Lower surface	
x/c	z/c	x/c	z/c
0	0	0	0
.00423	.00868	.00577	-.00756
.00664	.01058	.00836	-.00900
.01151	.01367	.01349	-.01125
.02384	.01944	.02616	-.01522
.04869	.02769	.05131	-.02047
.07364	.03400	.07636	-.02428
.09863	.03917	.10137	-.02725
.14869	.04729	.15131	-.03167
.19882	.05328	.20118	-.03468
.24898	.05764	.25102	-.03662
.29916	.06060	.30084	-.03764
.34935	.06219	.35065	-.03771
.39955	.06247	.40045	-.03689
.44975	.06151	.45025	-.03523
.49994	.05943	.50006	-.03283
.55012	.05637	.54988	-.02985
.60028	.05245	.59972	-.02641
.65041	.04772	.64959	-.02262
.70052	.04227	.69948	-.01861
.75061	.03624	.74939	-.01464
.80074	.02974	.79926	-.01104
.85072	.02254	.84928	-.00812
.90050	.01519	.89950	-.00539
.95026	.00769	.94974	-.00279
1.00000	.00021	1.00000	-.00021

Leading-edge radius 0.0077c

Slope of radius through leading edge 0.0842

TABLE II.- SINGLE-SLOTTED TRAILING-EDGE-FLAP COORDINATES PARALLEL TO THE MODEL PLANE OF SYMMETRY

Upper surface		Lower surface	
x/c	z/c	x/c	x/c
0	0	0	0
.0018	.0071	.0025	-.0042
.0062	.0120	.0050	-.0061
.0106	.0150	.0100	-.0085
.0221	.0193	.0175	-.0105
.0336	.0212	.0250	-.0115
.0460	.0221	.0325	-.0118
.0902	.0219	.0400	-.0115
.0990	.0217	.0493	-.0110
.1080	.0210	.0993	-.0081
.1505	.0152	.1495	-.0054
.2003	.0077	.1997	-.0028
.2500	.0002	.2500	-.0002

TABLE III.- FAN INLET COORDINATES

a, in.	Section B-B	[1]Section C-C	[1]Section D-D
	r, in.	r, in.	r, in.
0	44.18	38.05	36.53
.090	40.98	36.61	35.42
.450	38.36	35.34	34.25
.900	37.15	34.48	33.53
1.350	36.35	33.94	33.07
1.800	35.77	33.54	32.75
2.250	35.29	33.23	32.50
3.150	34.55	32.77	32.14
4.050	33.98	32.45	31.94
4.950	33.53	32.23	31.80
7.650	32.57	31.80	31.56
10.350	31.92	31.58	-----
11.250	-----	-----	31.50
13.050	31.58	31.50	↓
14.750	31.50	31.50	

[1]See figure 5(d).

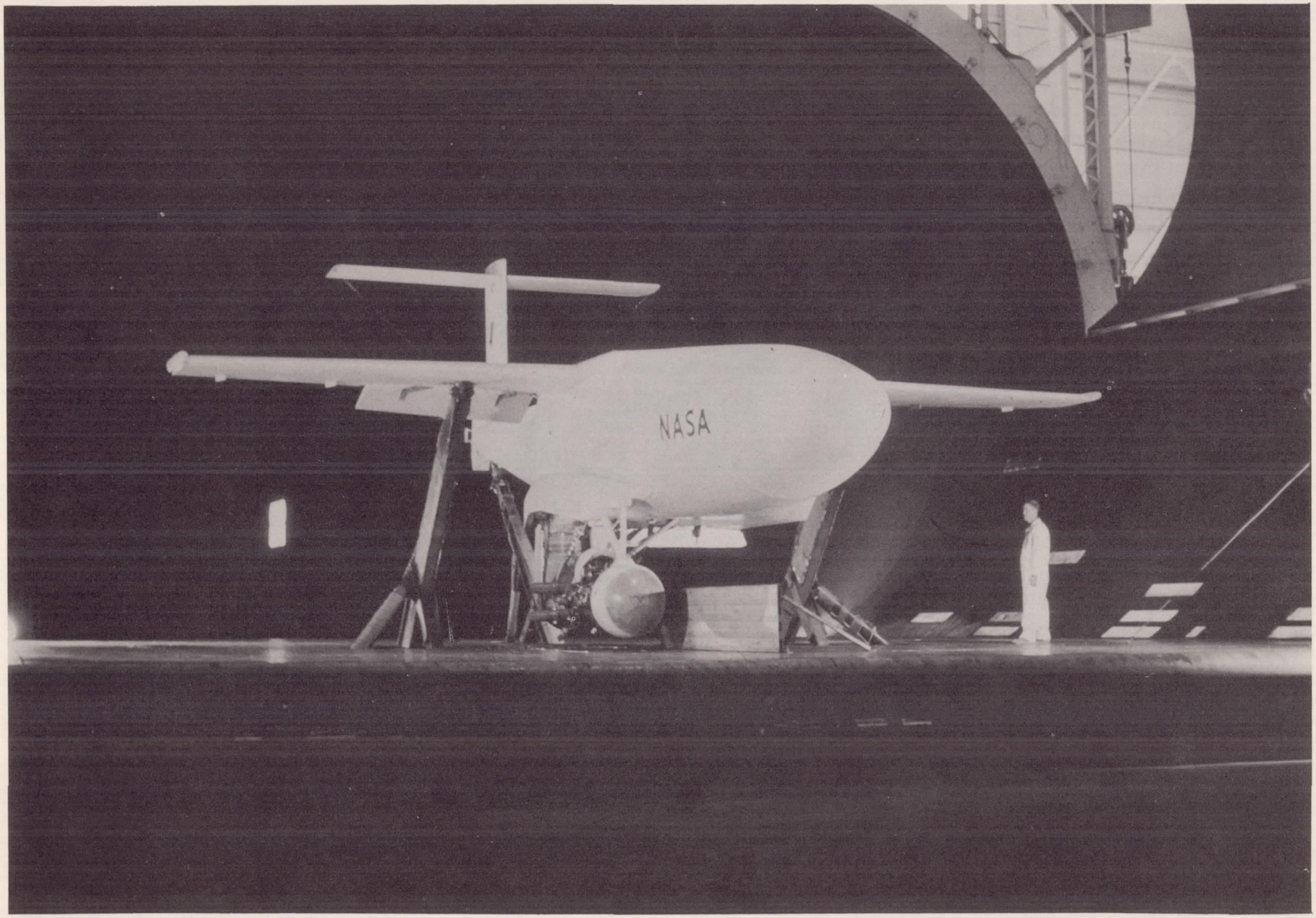

(a) Ground height h/d = 1.83.

A-27835

Figure 1.- Photographs of the model mounted on the variable height strut system in the Ames 40- by 80-Foot Wind Tunnel.

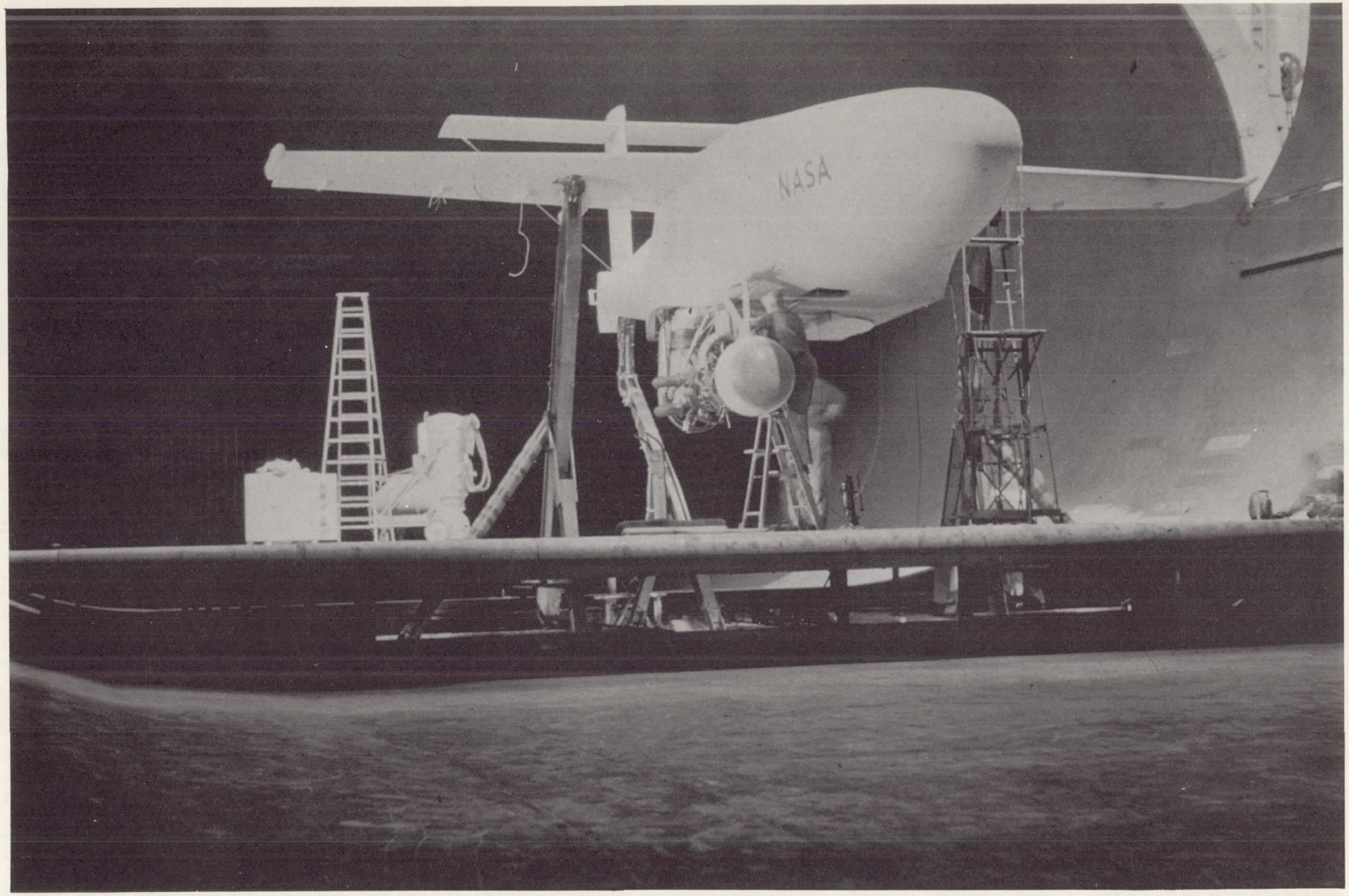

A-27831

(b) Ground height h/d = 2.39.

Figure 1.- Concluded

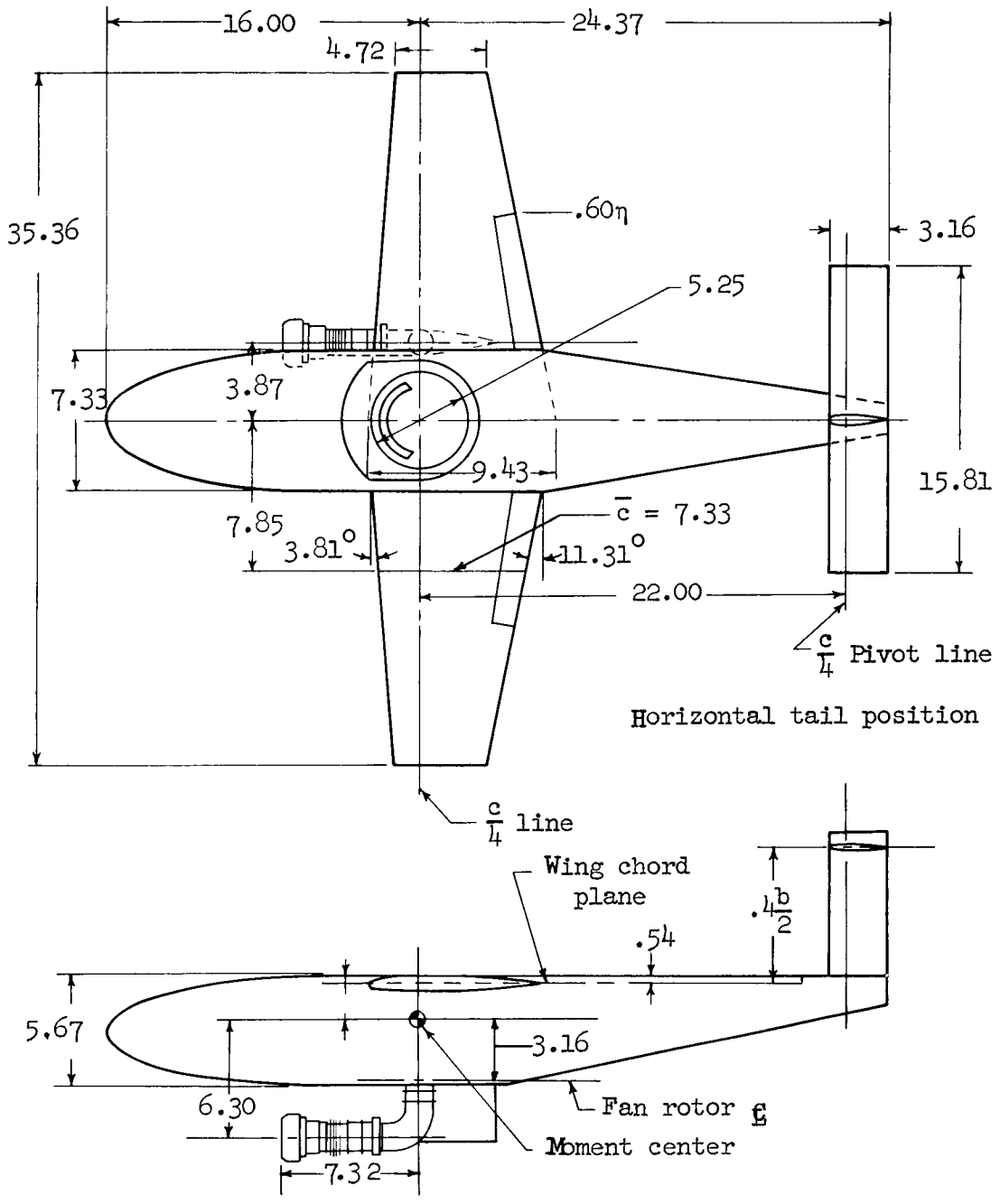

	Wing	Horizontal tail	Vertical tail
Area, sq ft	250	50	25
Aspect ratio	5.0	5.0	2.5
Taper ratio	0.5	1.0	1.0
Airfoil Section	NASA 63-210	NASA 63A012	NASA 63A015

Figure 2.- Geometric details of the model. (All dimensions in feet except as noted)

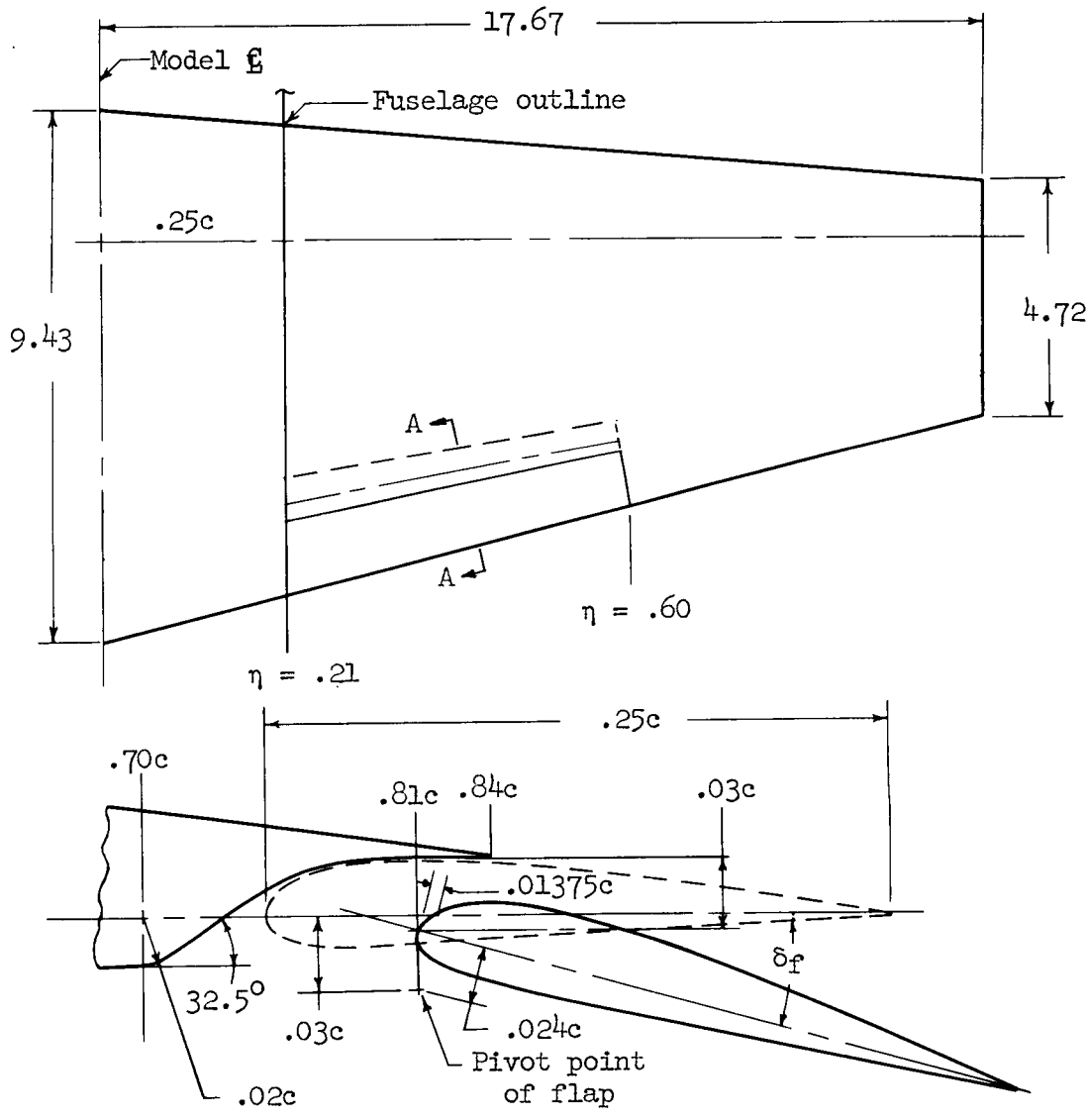

Section A-A

Figure 3.- Details of the trailing-edge flap.

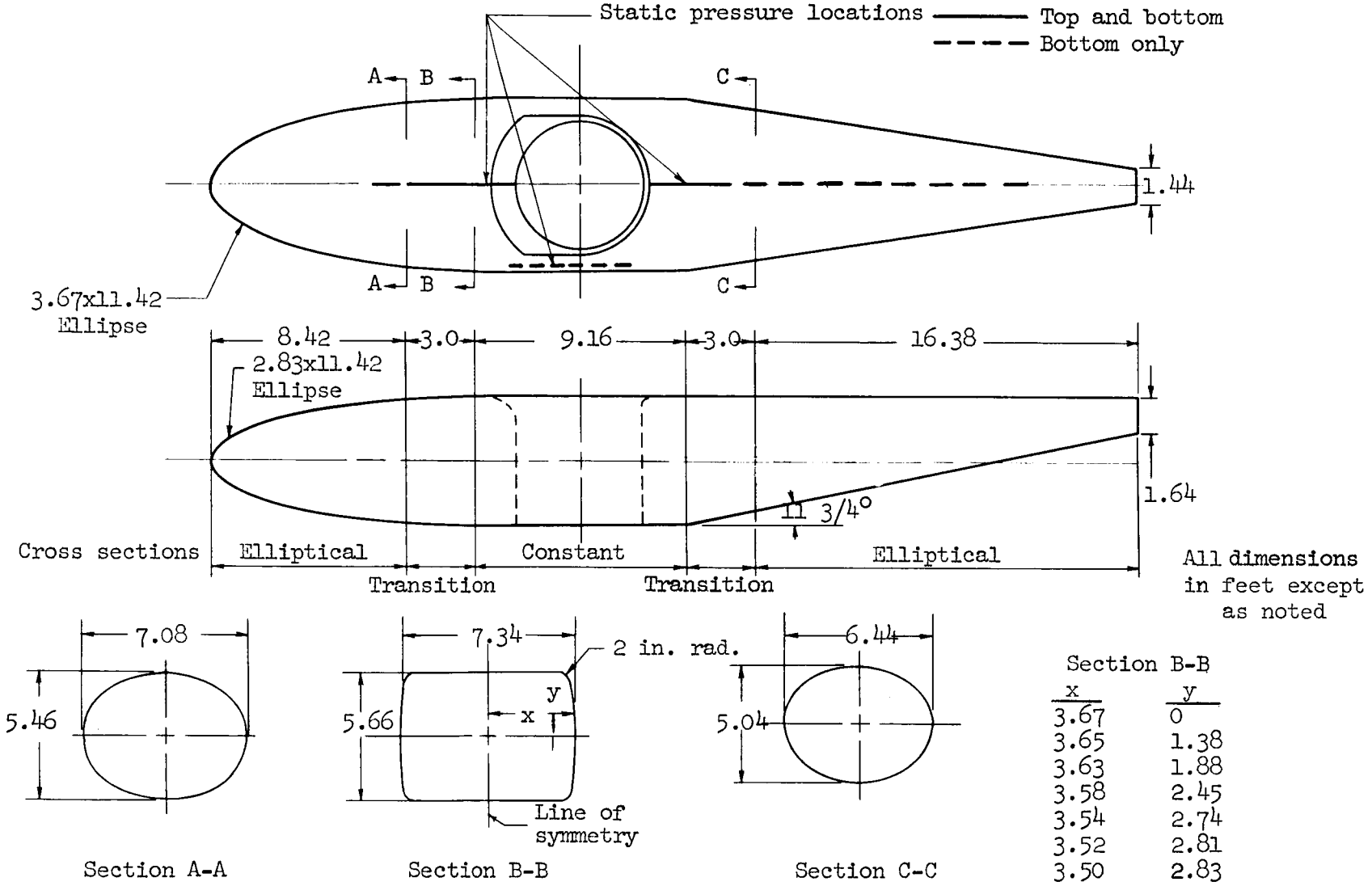

Section B-B

x	y
3.67	0
3.65	1.38
3.63	1.88
3.58	2.45
3.54	2.74
3.52	2.81
3.50	2.83

Figure 4.- Details of the fuselage.

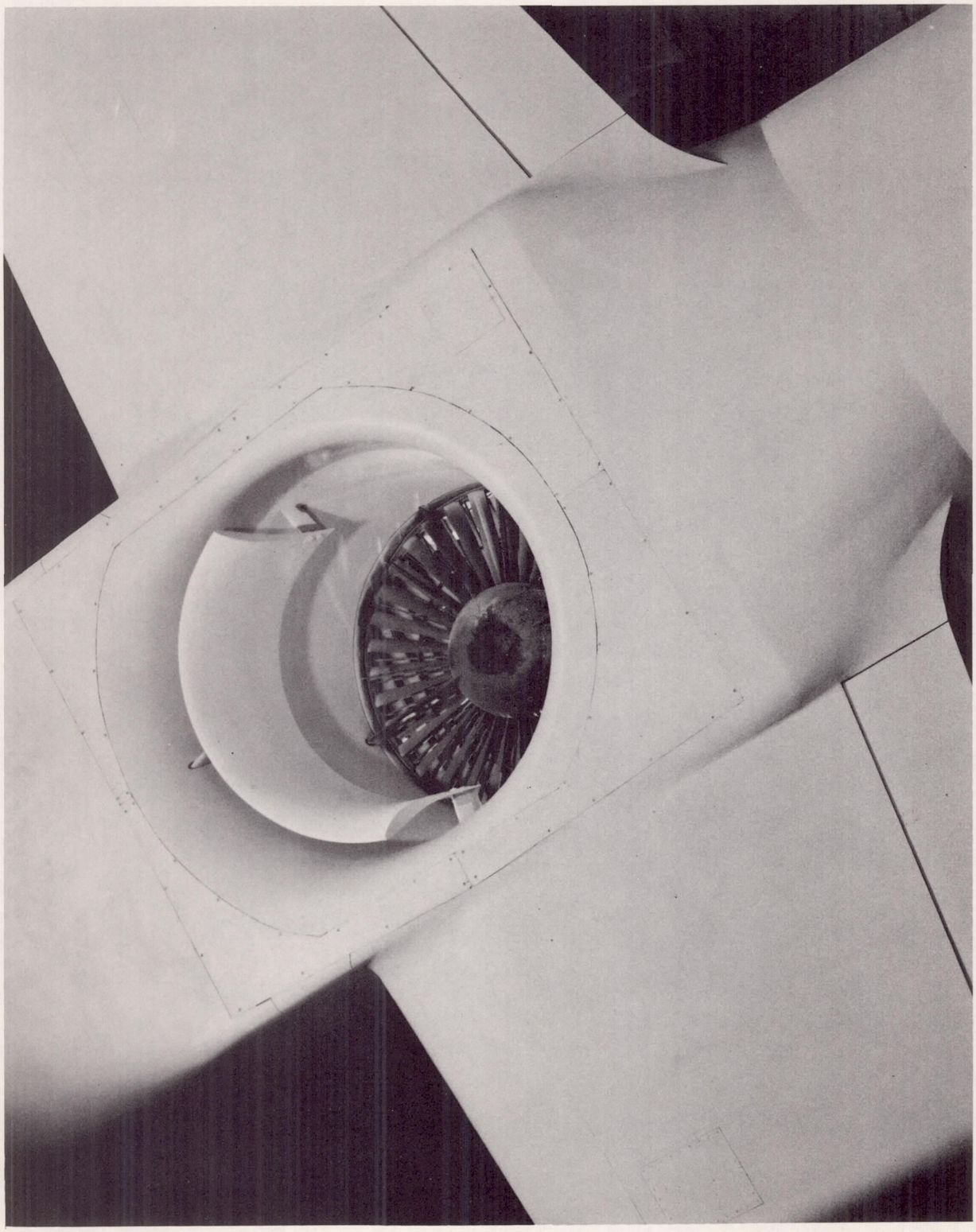

A-26763

(a) View of fan inlet.

Figure 5.- Details of the fan installation.

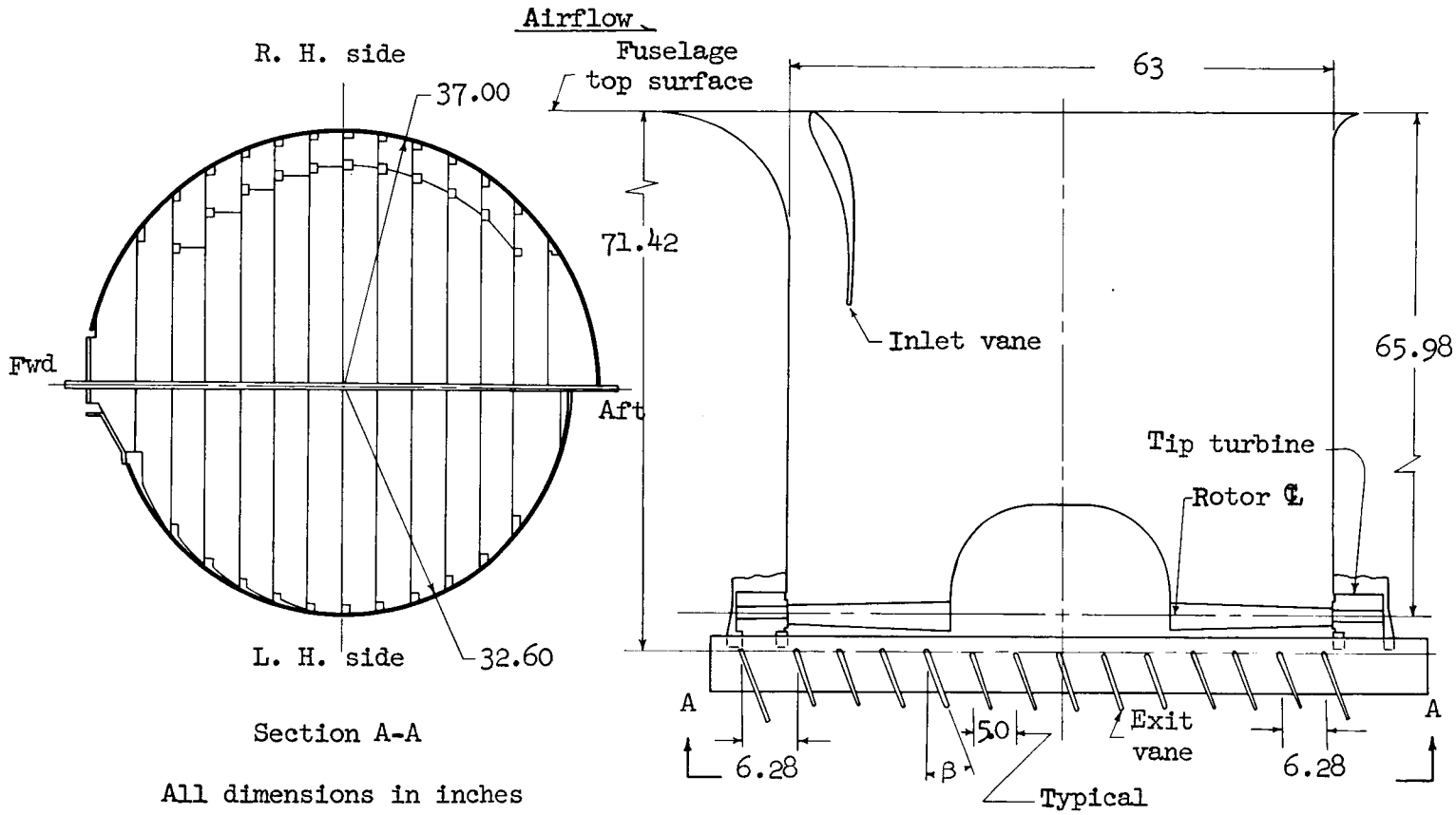

(b) Inlet duct and exit vane arrangement.

Figure 5.- Continued.

All dimensions in inches except as noted

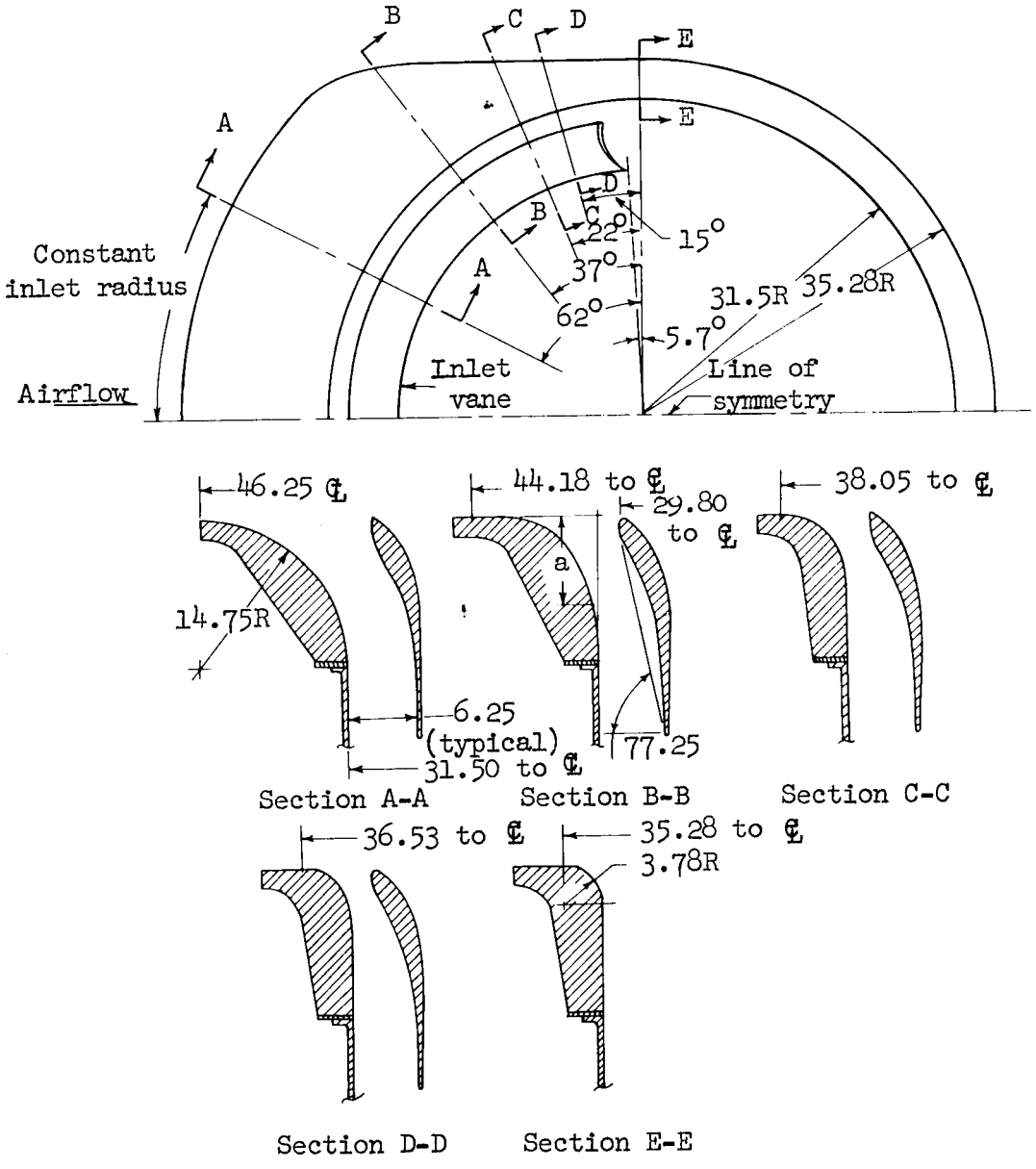

See table III for coordinates

(c) Details of inlet and inlet vane.

Figure 5.- Concluded.

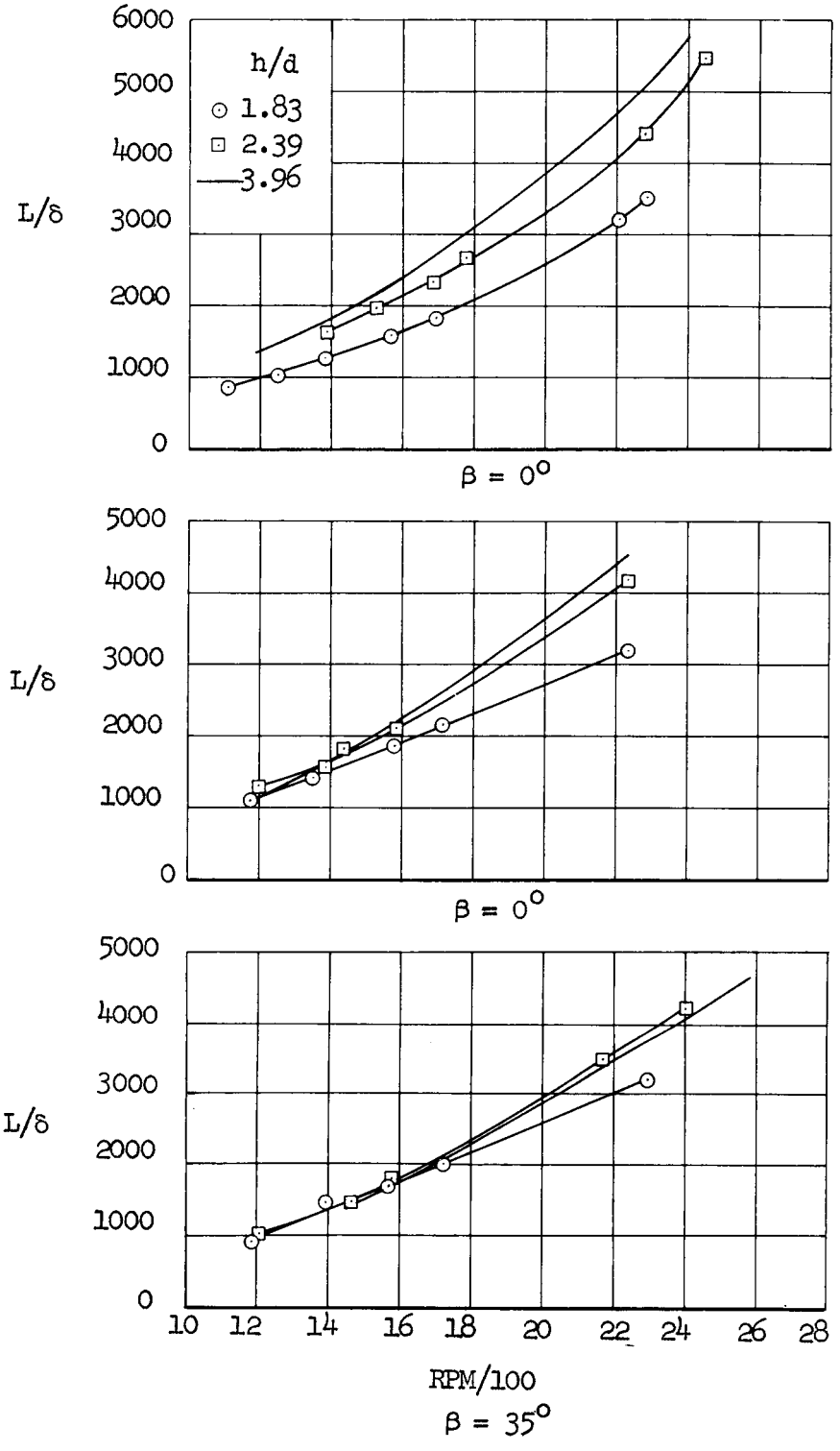

Figure 6.- Estimated zero airspeed total lift of the model, $\alpha = 0$.

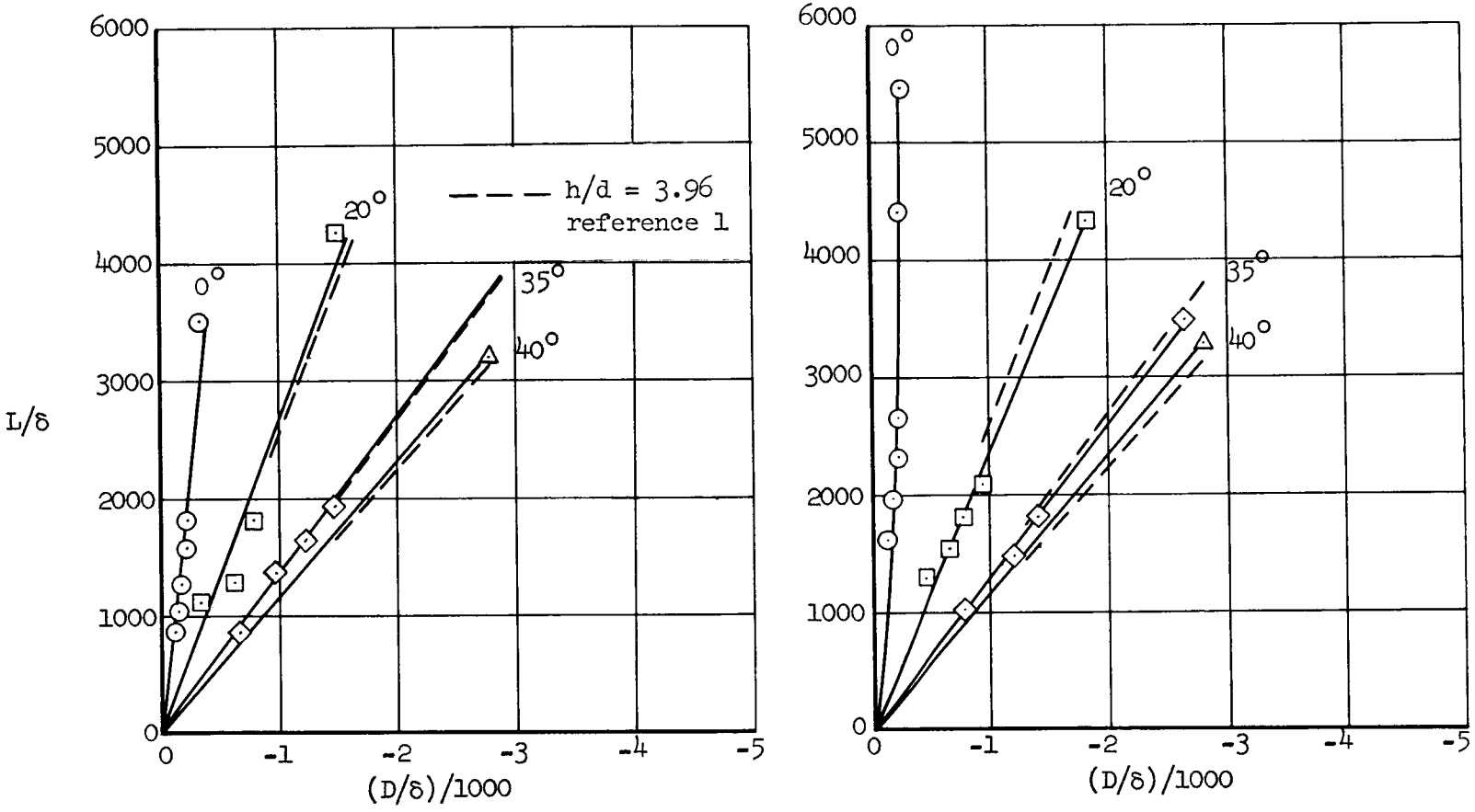

(a) h/D = 1.83

(b) h/D = 2.39

Figure 7.- Estimated zero airspeed characteristics of the model, 1100 - 2450 RPM; $\alpha = 0^{\circ}$.

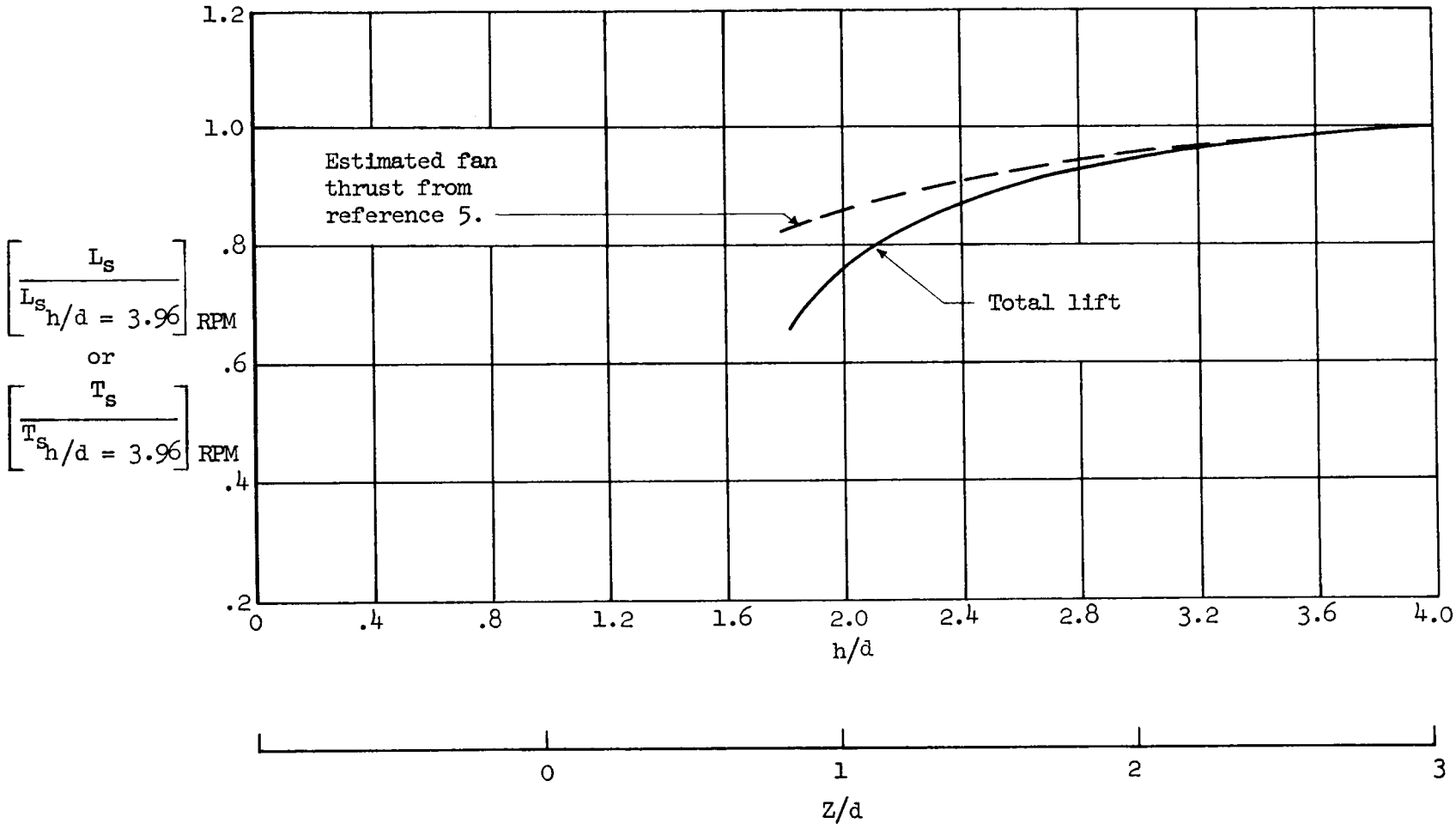

Figure 8.- Estimated effect of ground proximity on static lift; 2200 RPM, V = 0, $\beta = 0^{\circ}$, tail on.

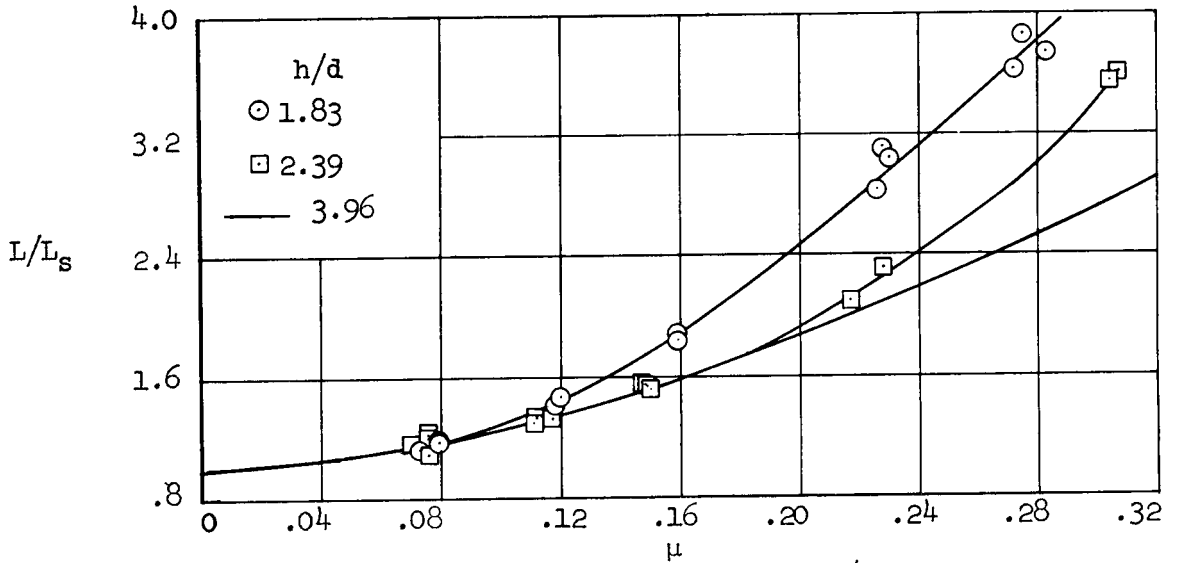

(a) L_s at appropriate h/d

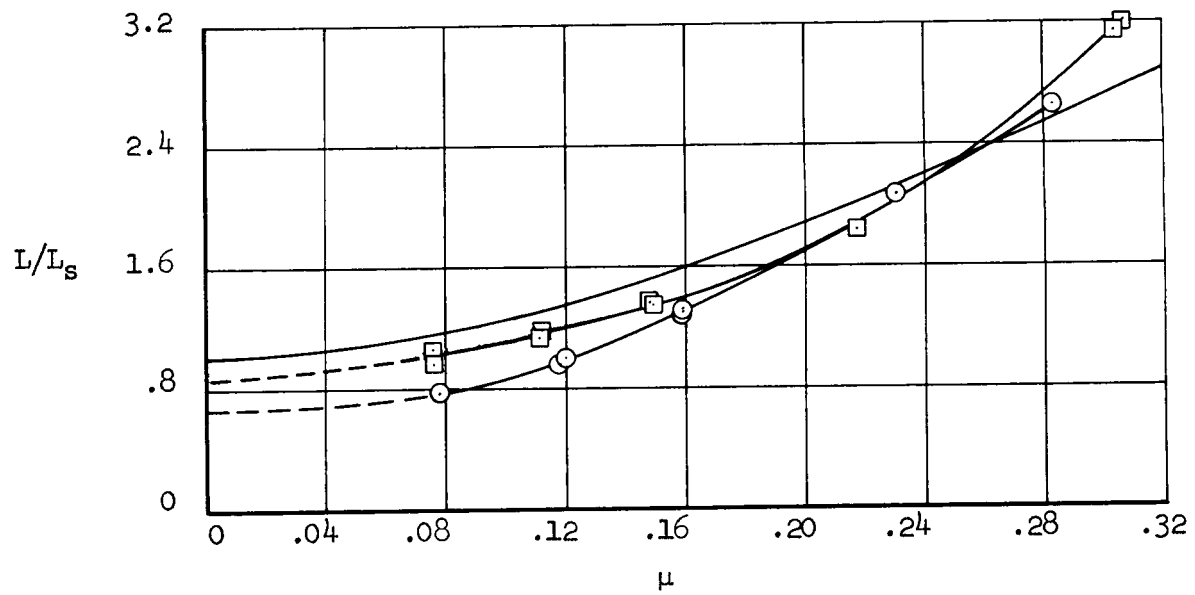

(b) L_s at h/d = 3.96

Figure 9.- Effect of forward speed on lift; 1700 RPM, $\alpha = 0^{\circ}$, $\beta = 0^{\circ}$, $\delta_f = 30^{\circ}$.

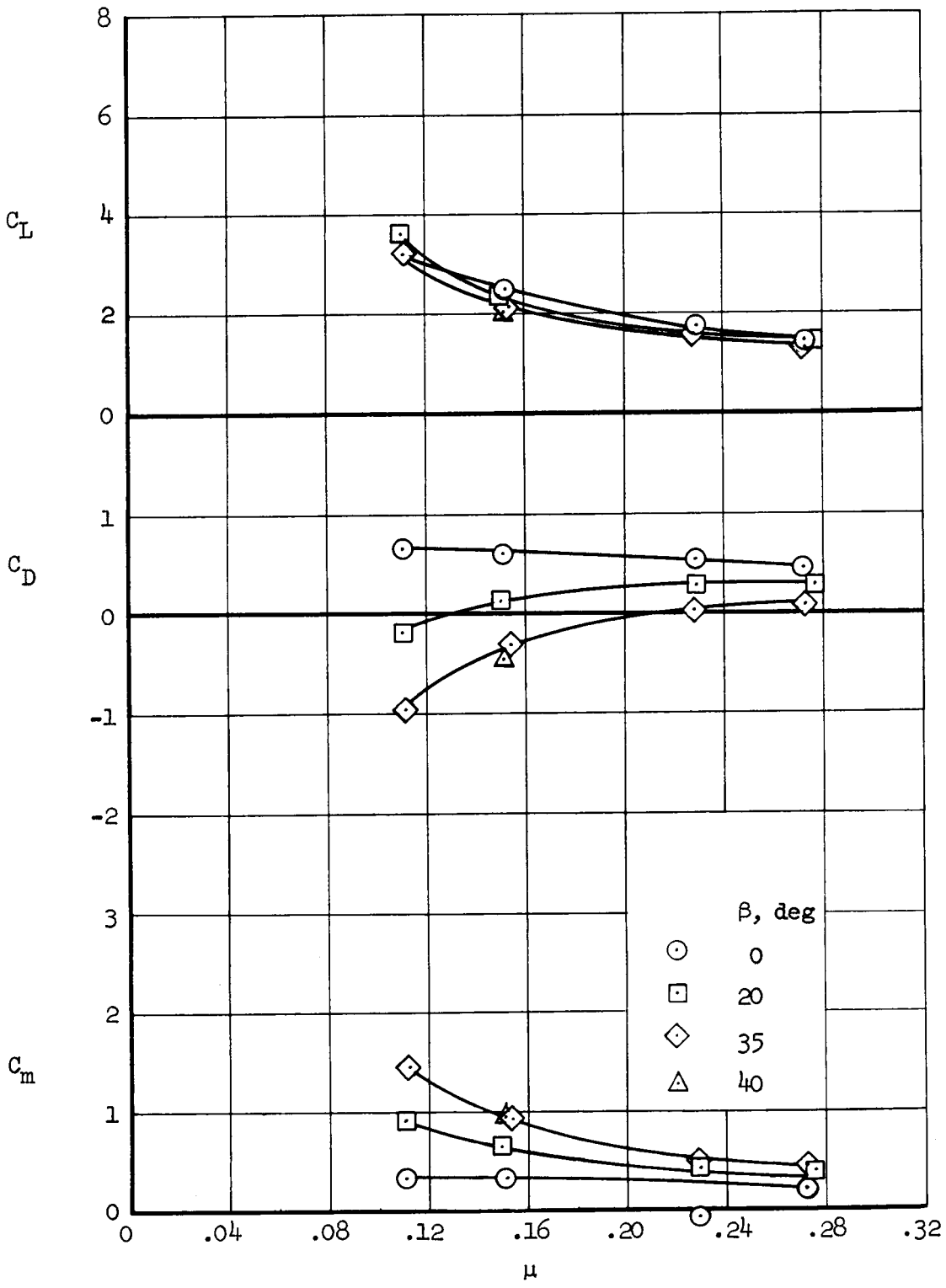

(a) h/d = 1.83

Figure 10.- Variation of longitudinal characteristics with tip-speed ratio, tail off, $\alpha = 0^{\circ}$, 1700 RPM.

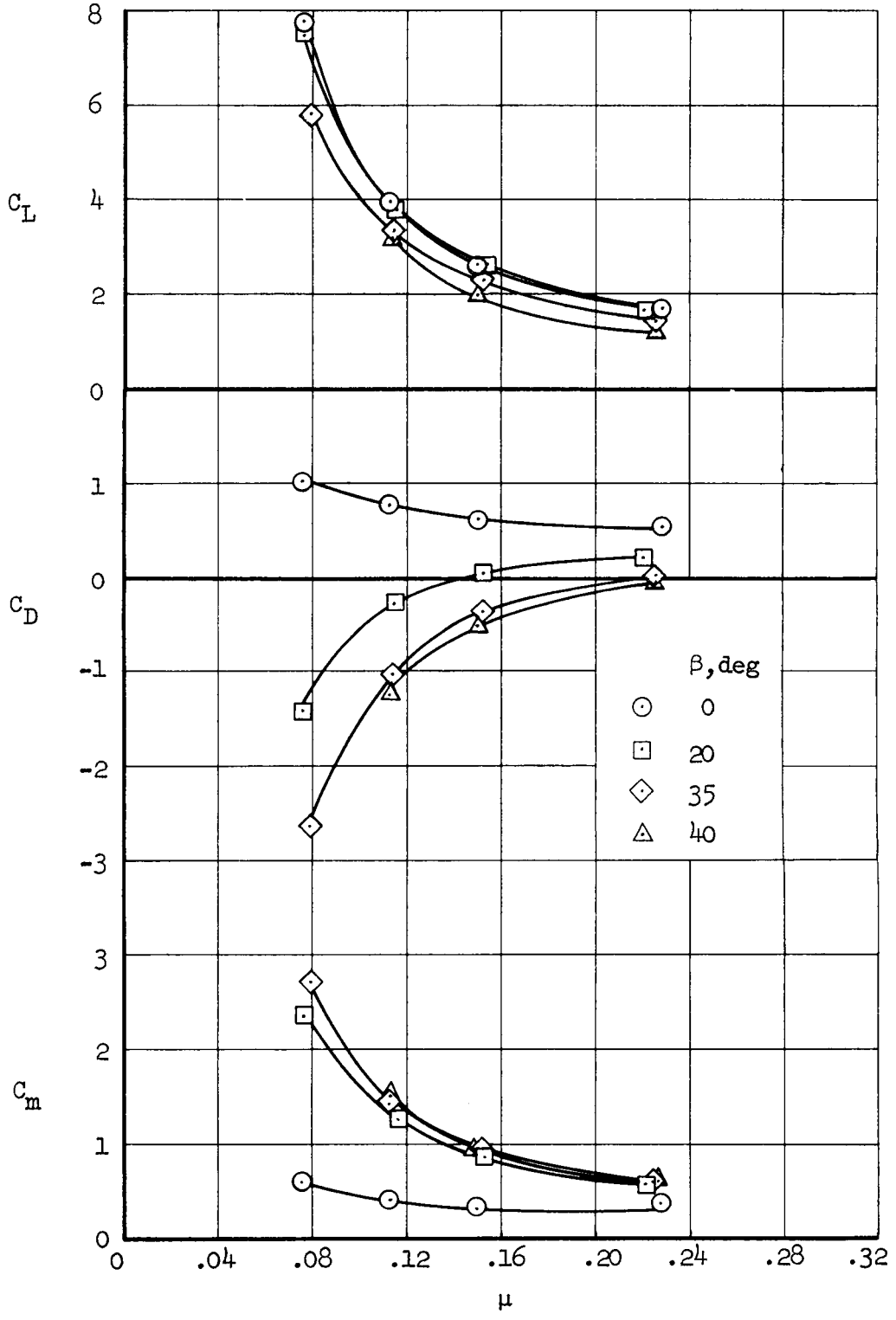

(b) h/d = 2.39

Figure 10.- Concluded.

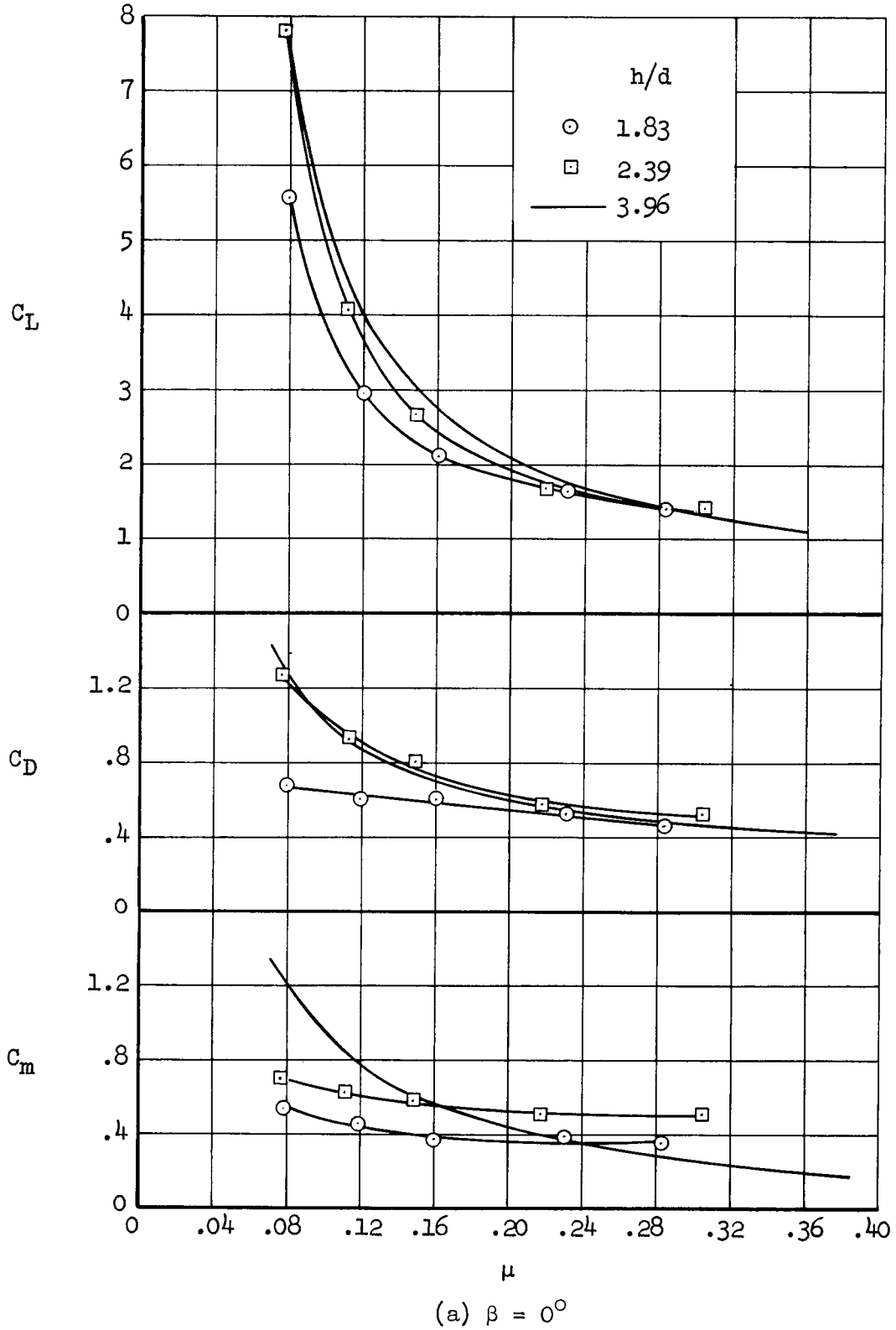

(a) $\beta = 0^\circ$

Figure 11.- Variation of longitudinal characteristics with tip-speed ratio, tail on, 1700 RPM, $\alpha = 0^\circ$, $\delta_f = 30^\circ$.

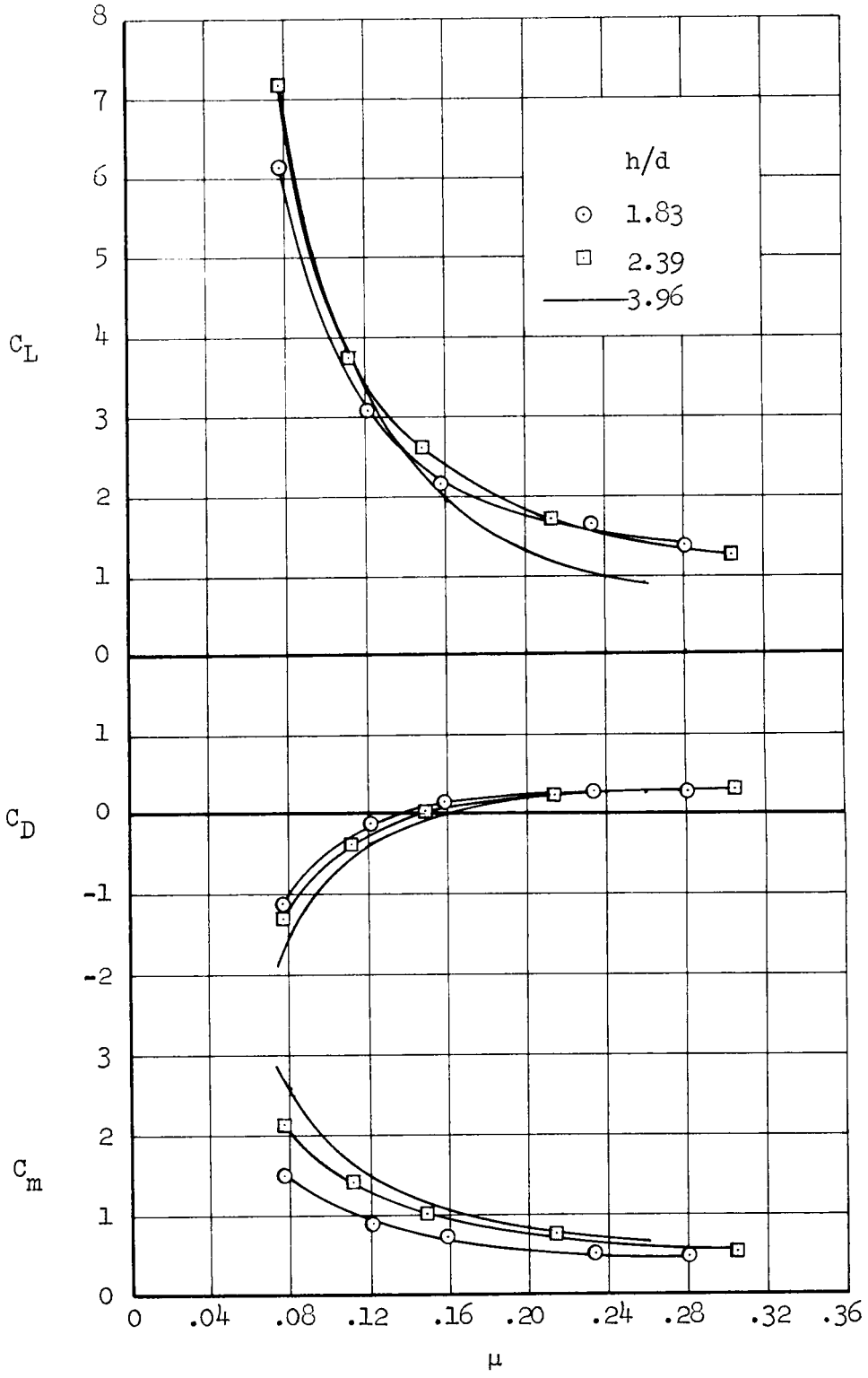

(b) $\beta = 20^{\circ}$

Figure 11.- Continued.

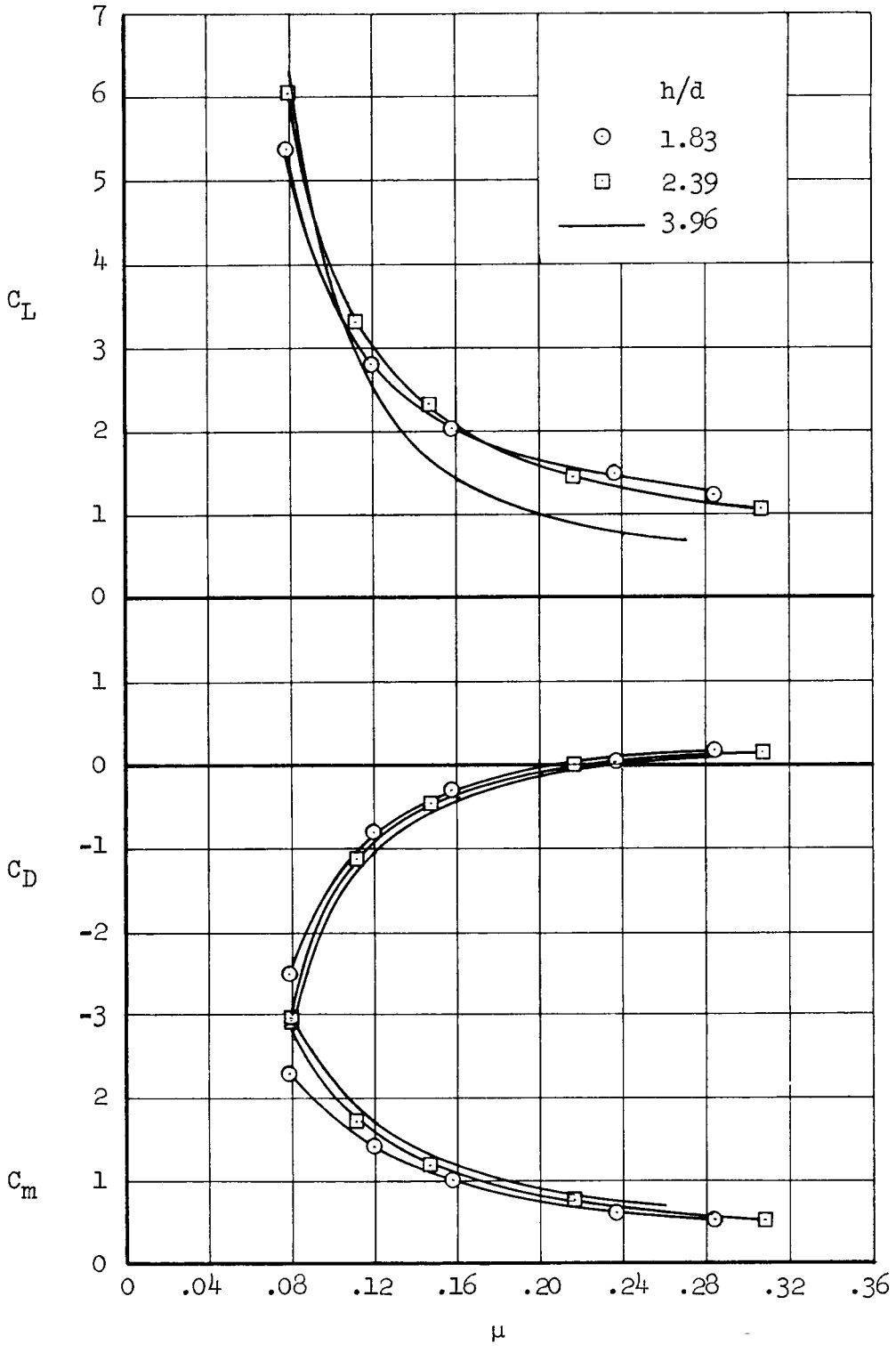

(c) $\beta = 35^\circ$

Figure 11.- Concluded.

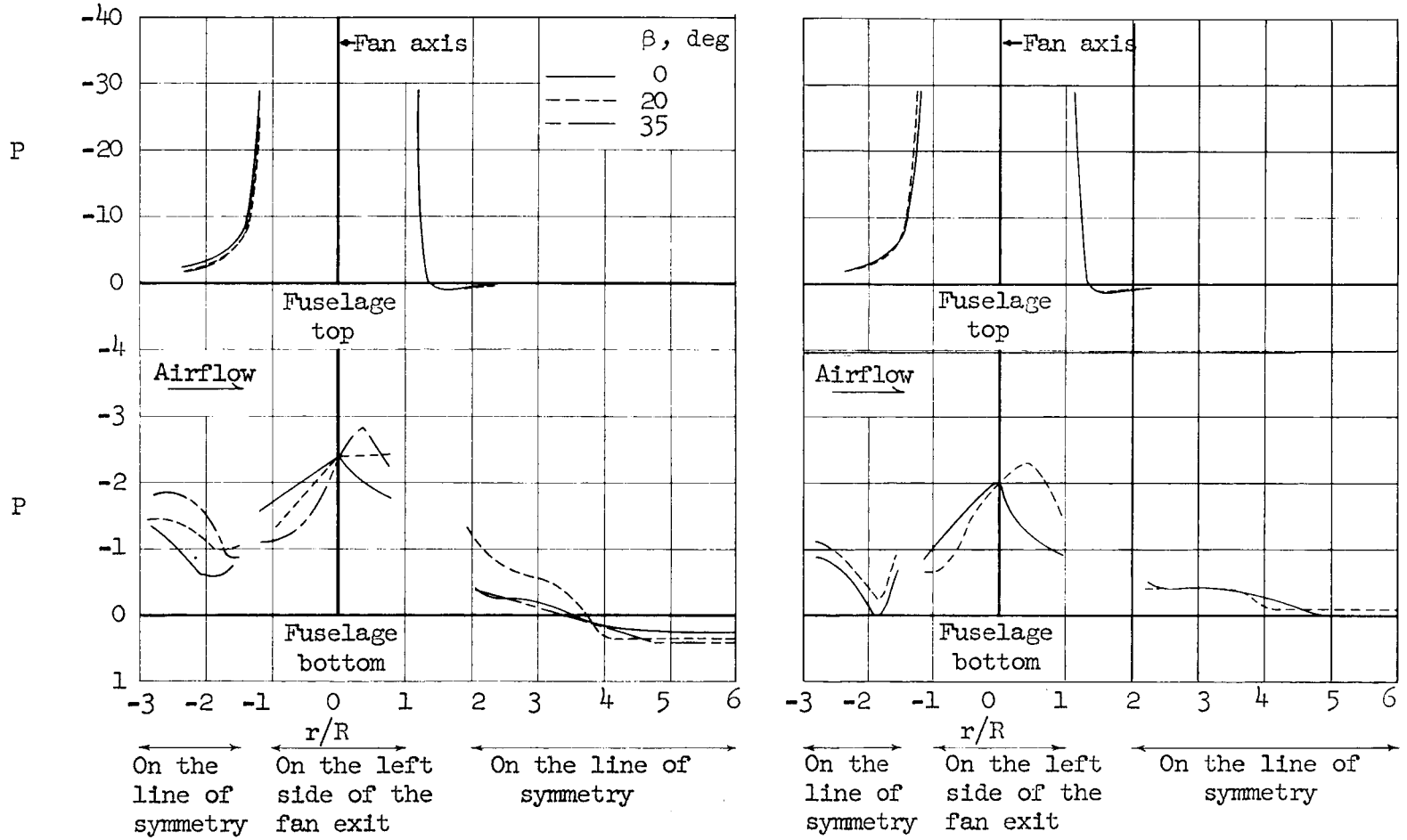

(a) h/d = 1.83, μ = 0.074

(b) h/d = 2.39, μ = 0.076

Figure 12.- Fuselage pressure distributions; $\alpha = 0^{\circ}$, 1700 RPM, V_{∞} = 20 knots.

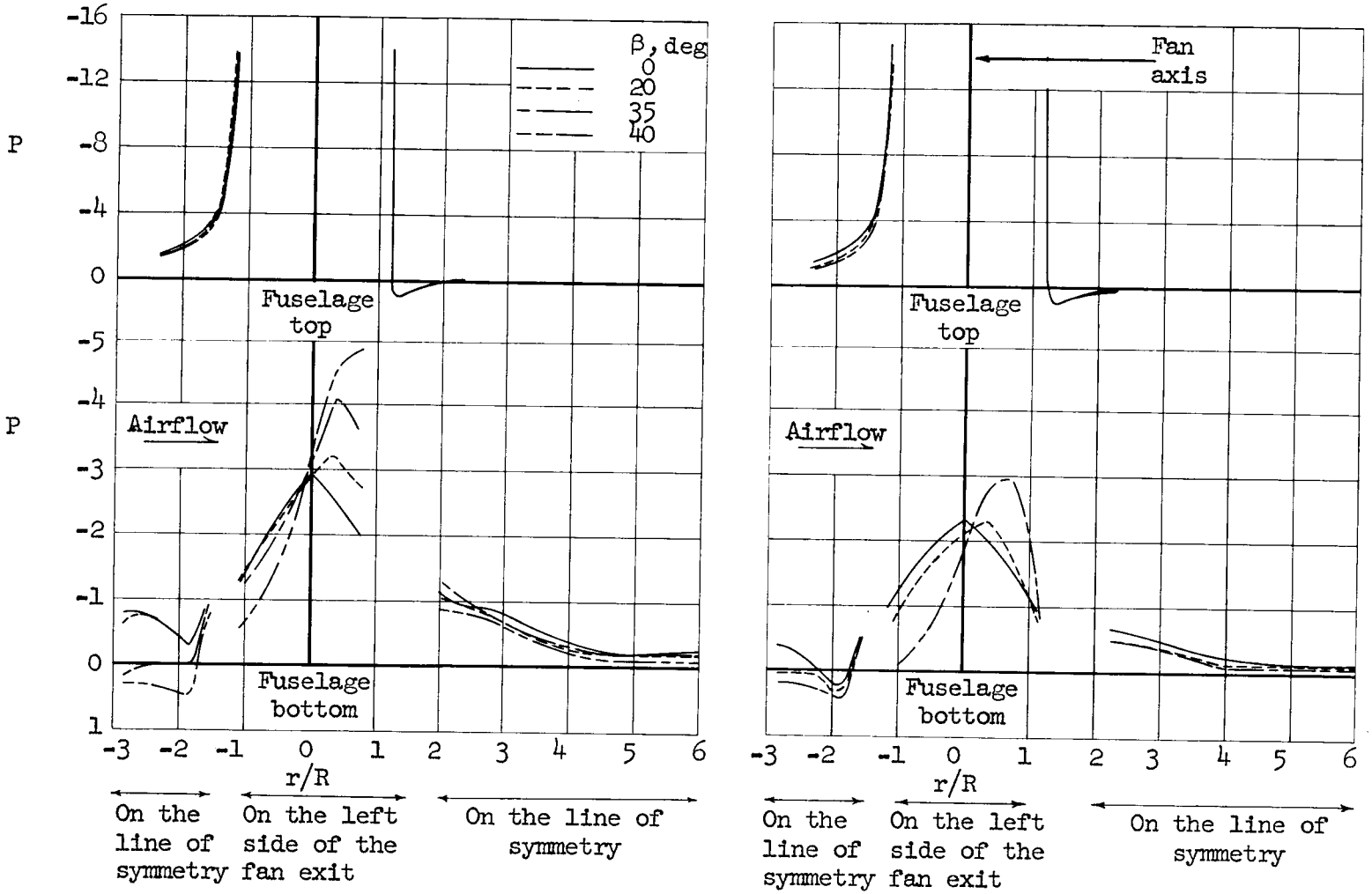

(a) h/d = 1.83, μ = 0.151

(b) h/d = 2.39, μ = 0.148

Figure 13.- Longitudinal pressure distributions on the fuselage; $\alpha = 0^{\circ}$, 1700 RPM, V_{∞} = 40 knots.

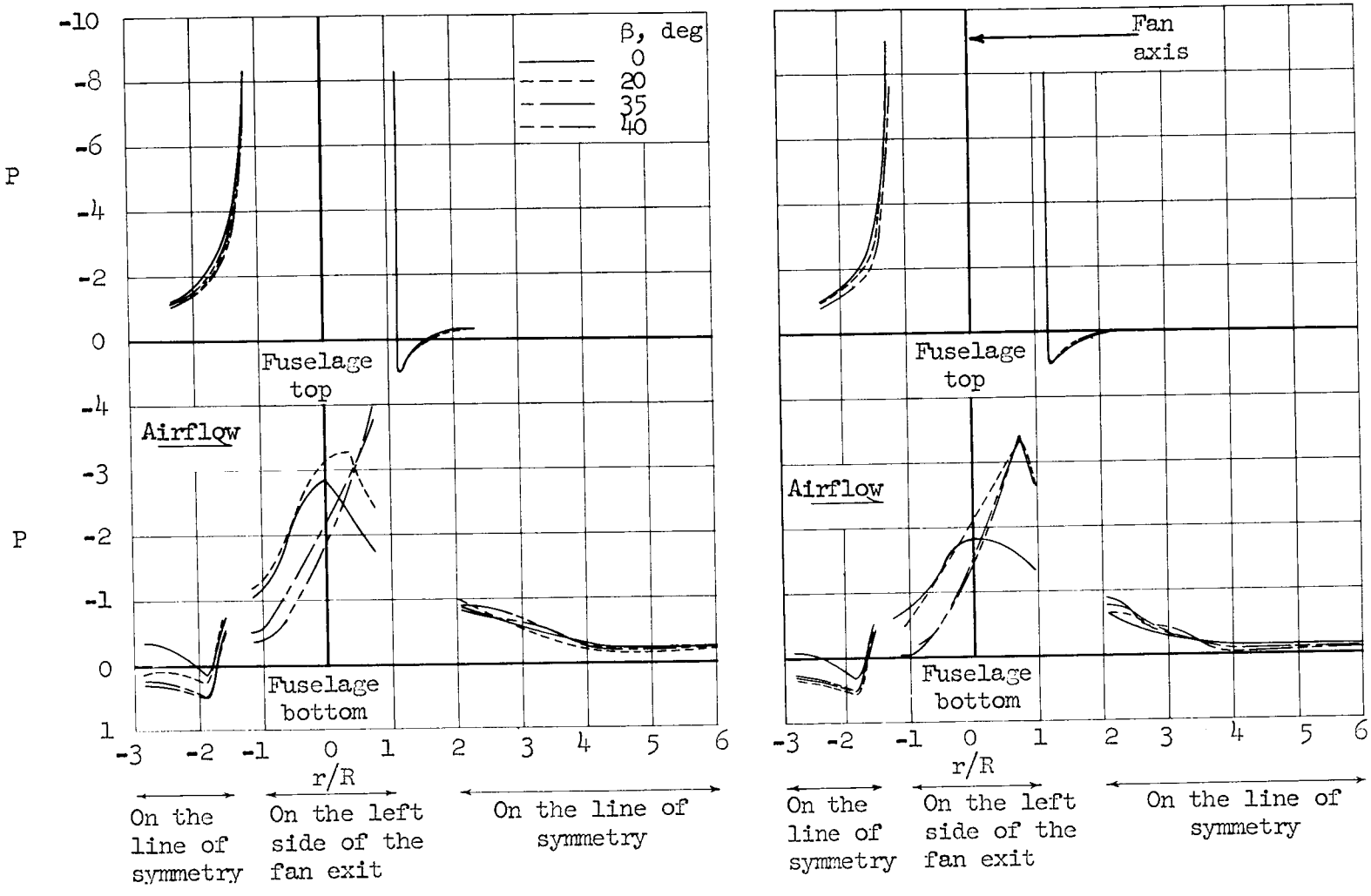

(a) h/d = 1.83, μ = 0.224

(b) h/d = 2.39, μ = 0.214

Figure 14.- Longitudinal pressure distributions on the fuselage, $\alpha = 0^{\circ}$, 1700 RPM, V_{∞} = 60 knots.

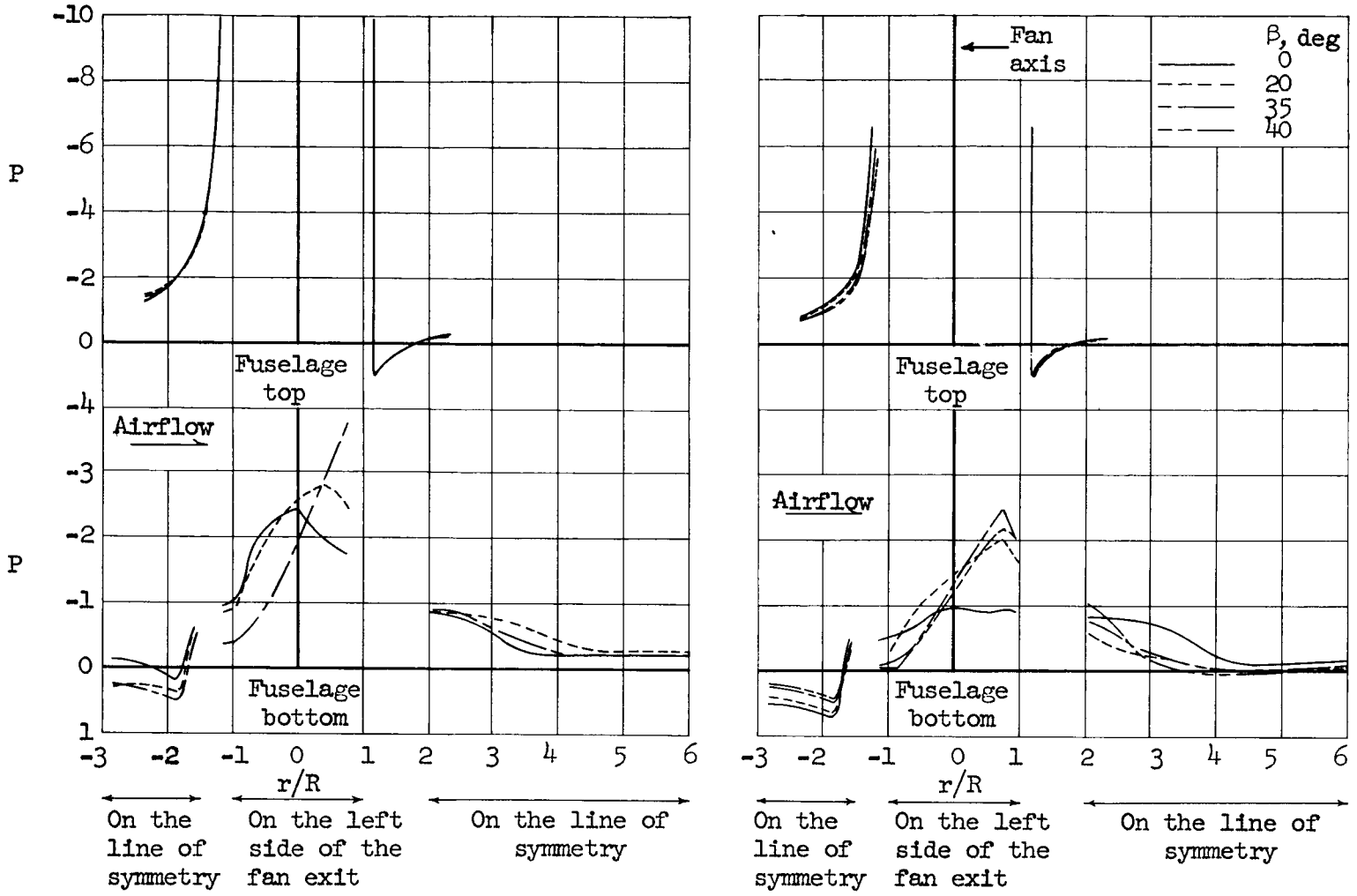

(a) h/d = 1.83, μ = 0.270, 1400 RPM, V_∞ = 60 knots

(b) h/d = 2.39, μ = 0.305, 1700 RPM, V_∞ = 80 knots

Figure 15.- Longitudinal pressure distribution on the fuselage, $\alpha = 0^\circ$.

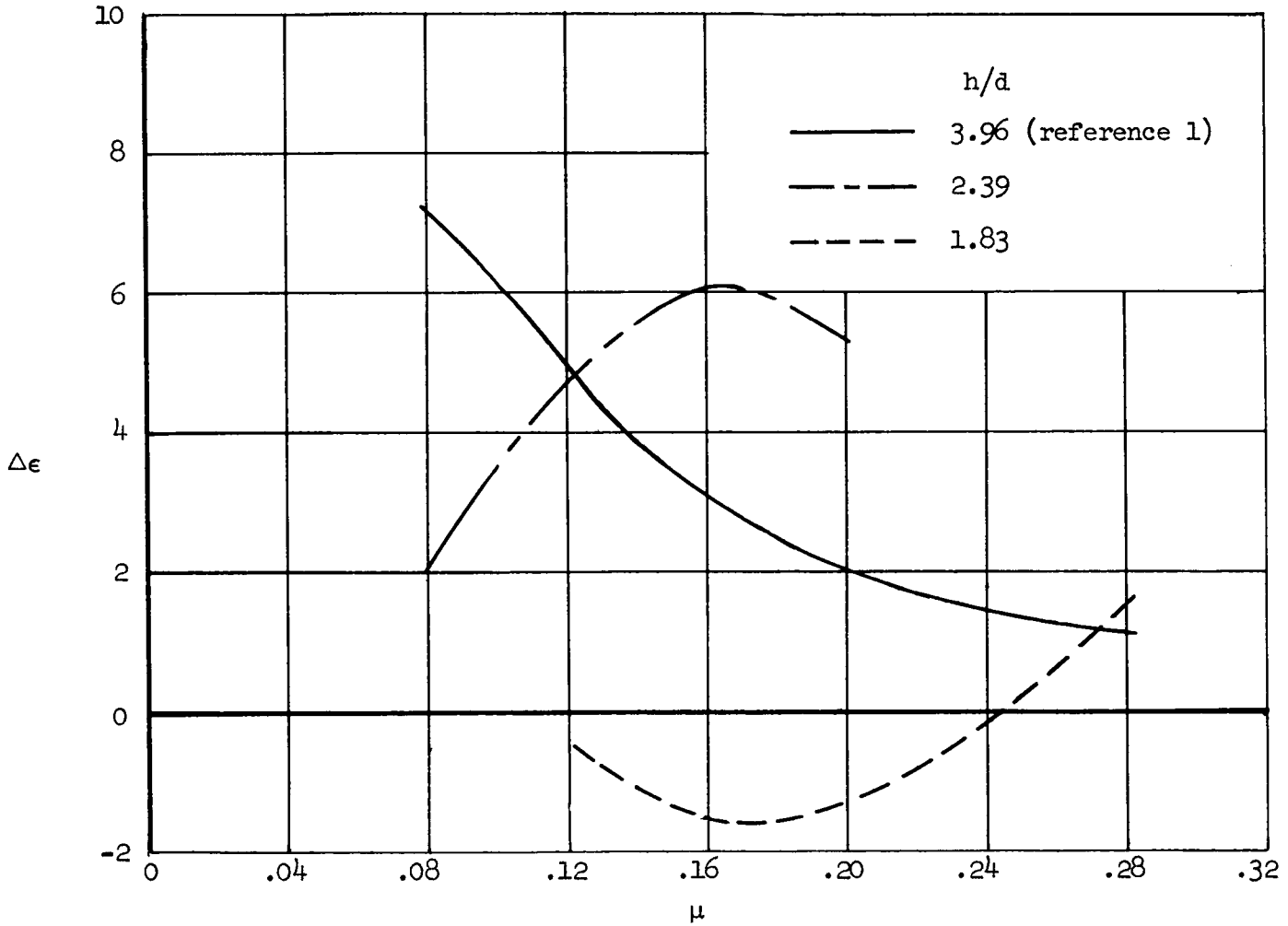

Figure 16.- Variation of average downwash at the horizontal tail due to fan operation with tip-speed ratio, $\alpha = 0^{\circ}$, high tail position.

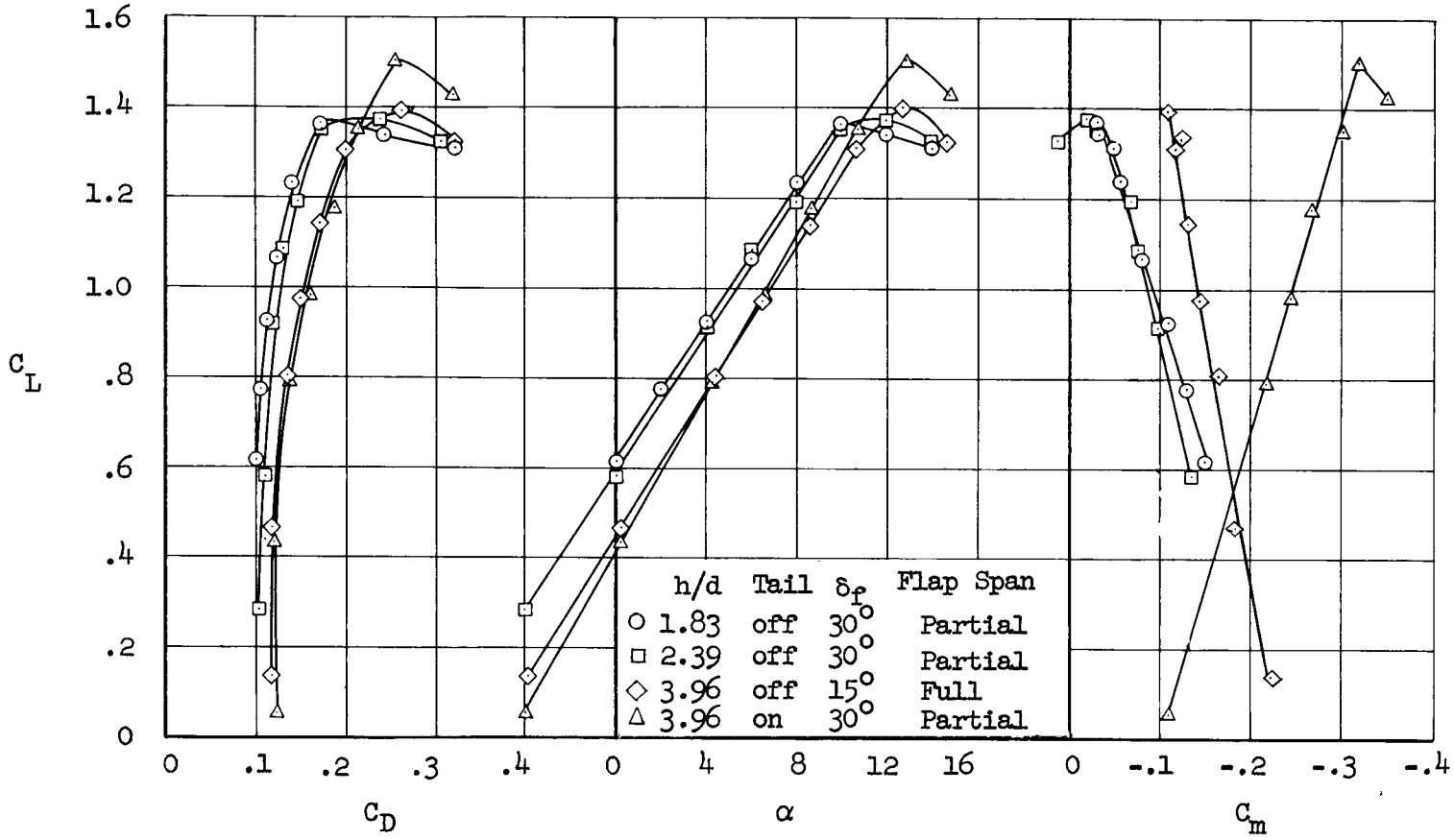

Figure 17.- Power-off longitudinal characteristics; duct closed, V_∞ = 60 knots.

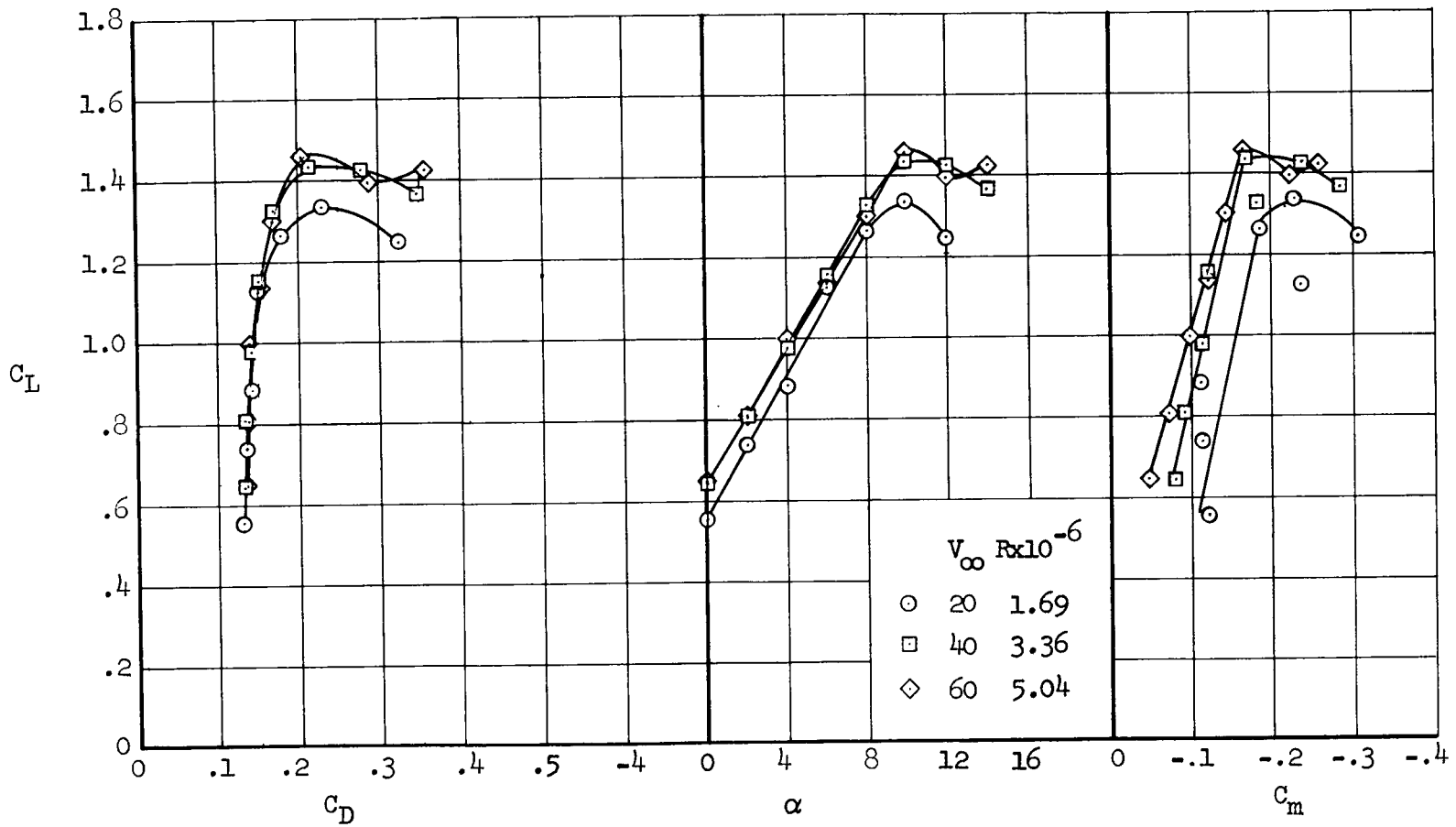

(a) h/d = 1.83

Figure 18.- Power-off longitudinal characteristics; inlet closed, tail on, $\delta_f = 30^\circ$.

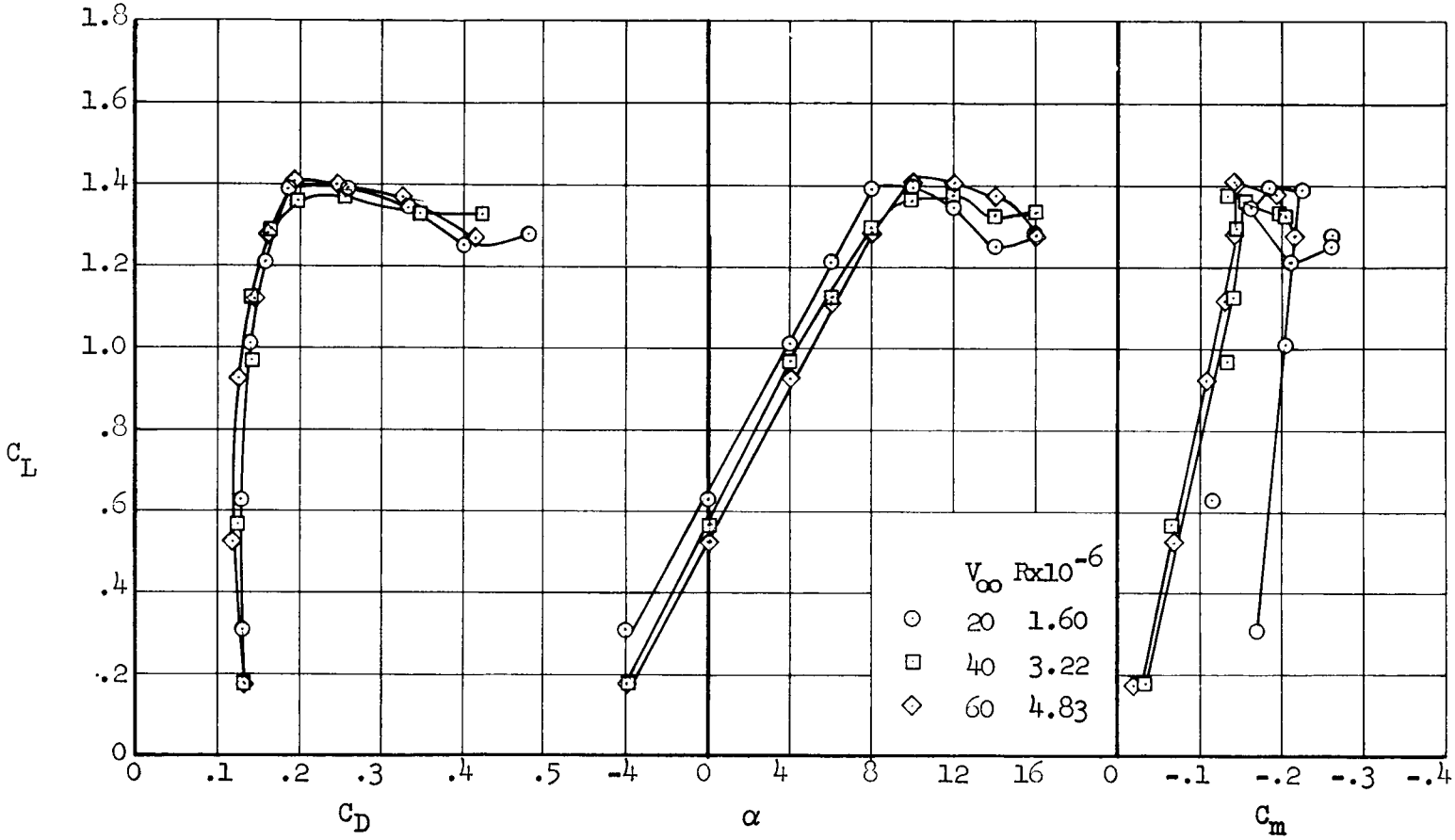

(b) h/d = 2.39

Figure 18.- Concluded.

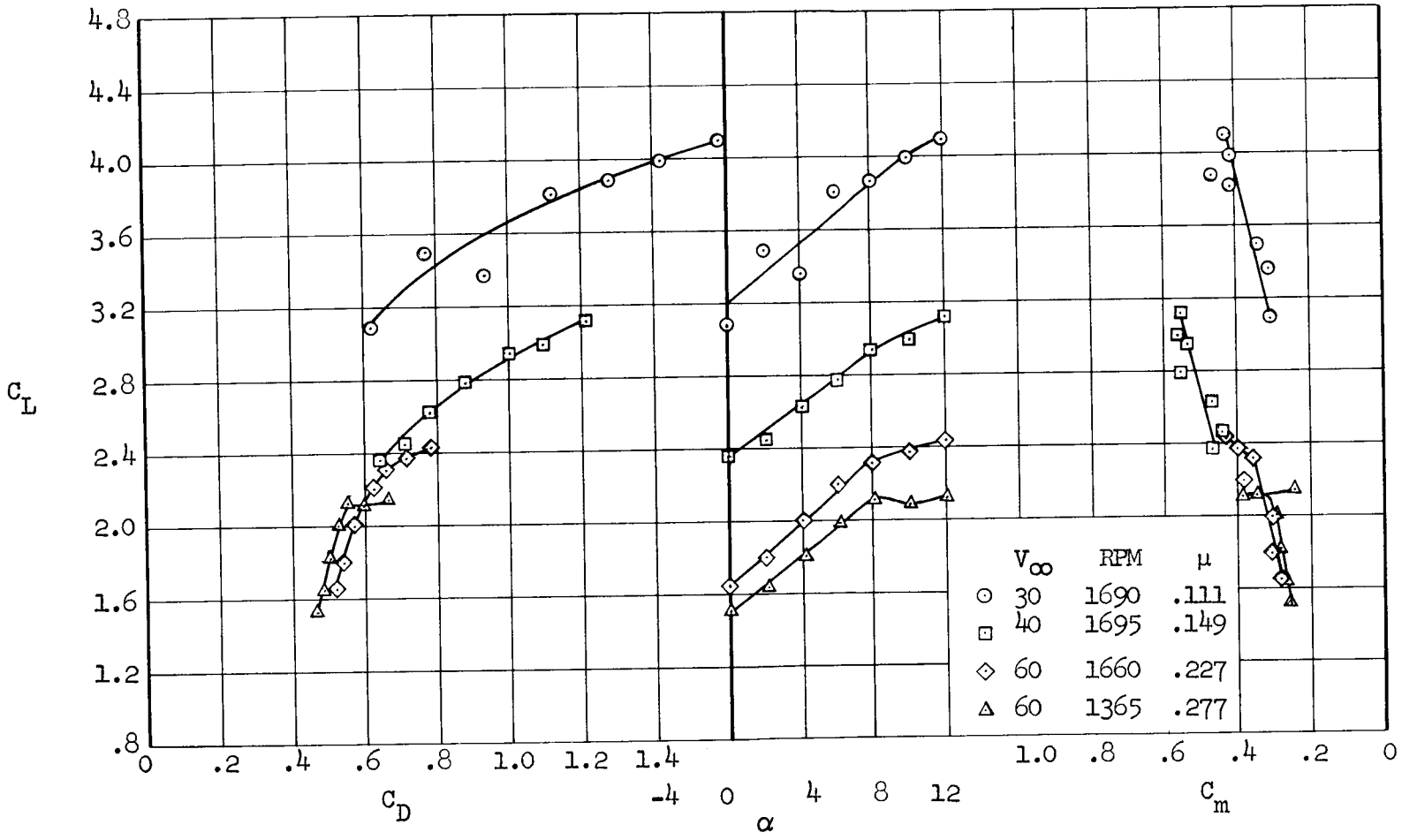

(a) h/d = 1.83

Figure 19.- Longitudinal characteristics with the horizontal tail off; $\delta_f = 30^\circ$, $\beta = 0^\circ$.

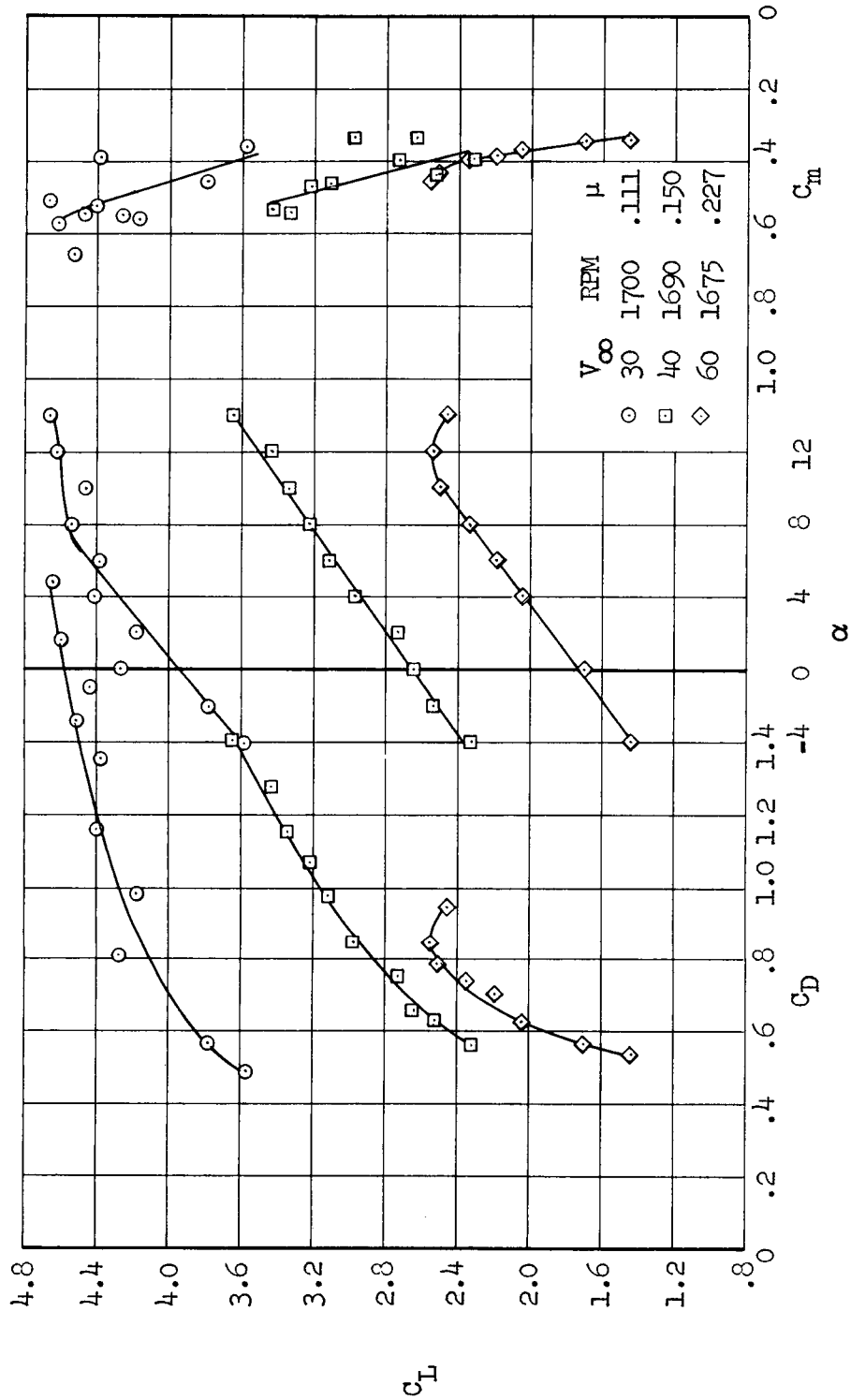

(b) h/d = 2.39

Figure 19.- Concluded.

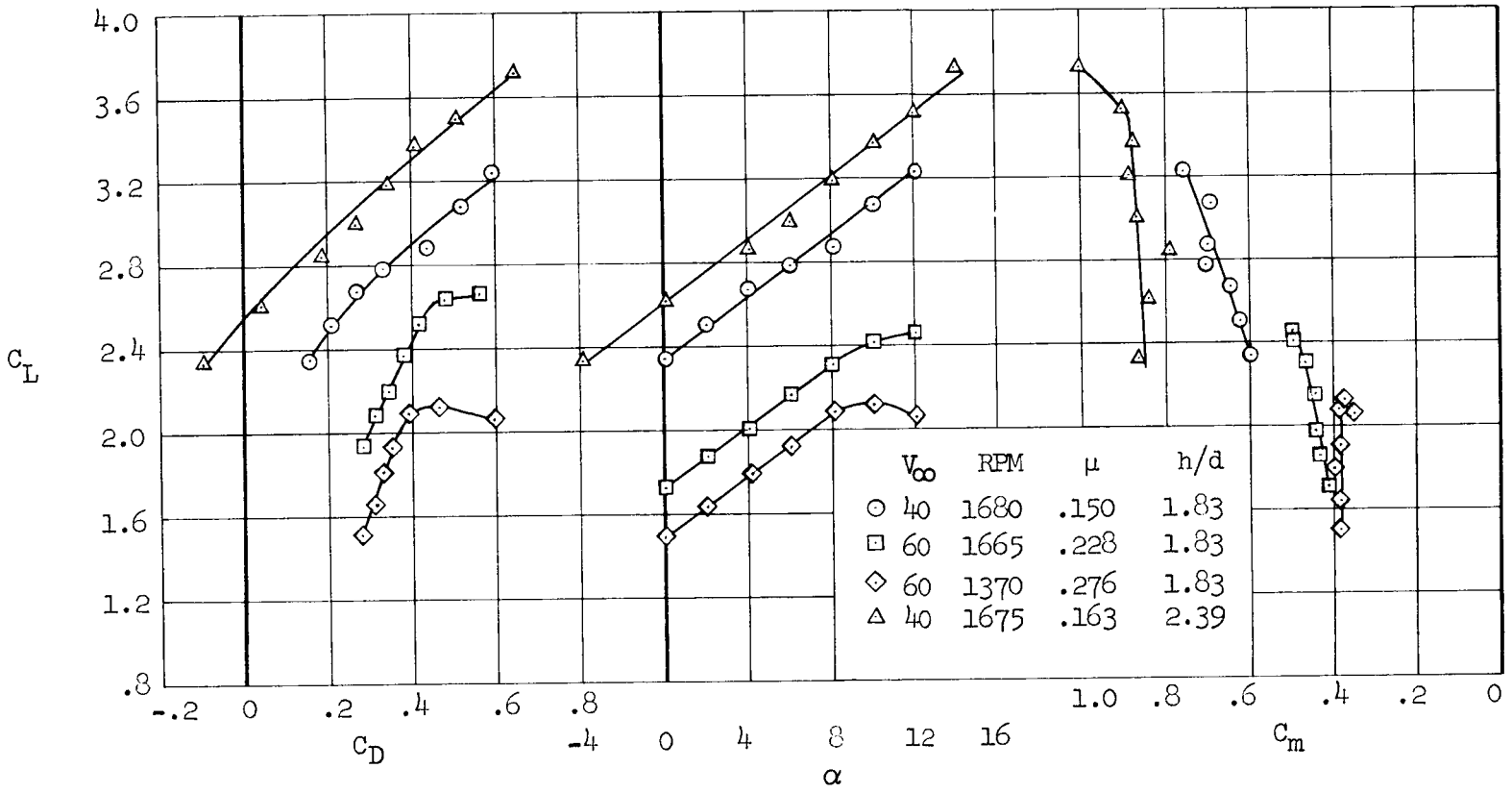

Figure 20.- Longitudinal characteristics with the horizontal tail off; $\delta_f = 30^\circ$, $\beta = 20^\circ$.

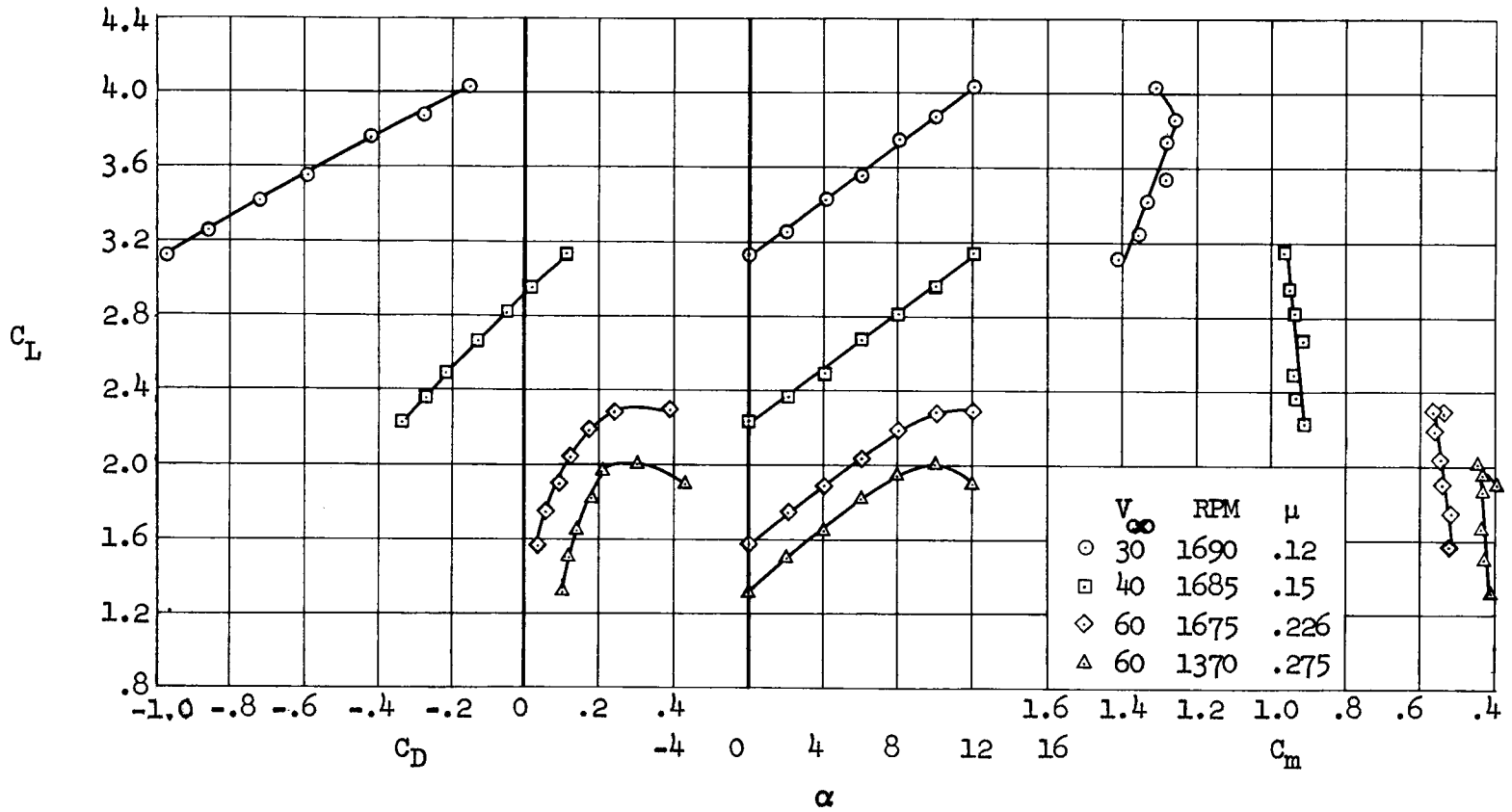

(a) h/d = 1.83

Figure 21.- Longitudinal characteristics with the tail off; $\delta_f = 30^\circ$, $\beta = 35^\circ$.

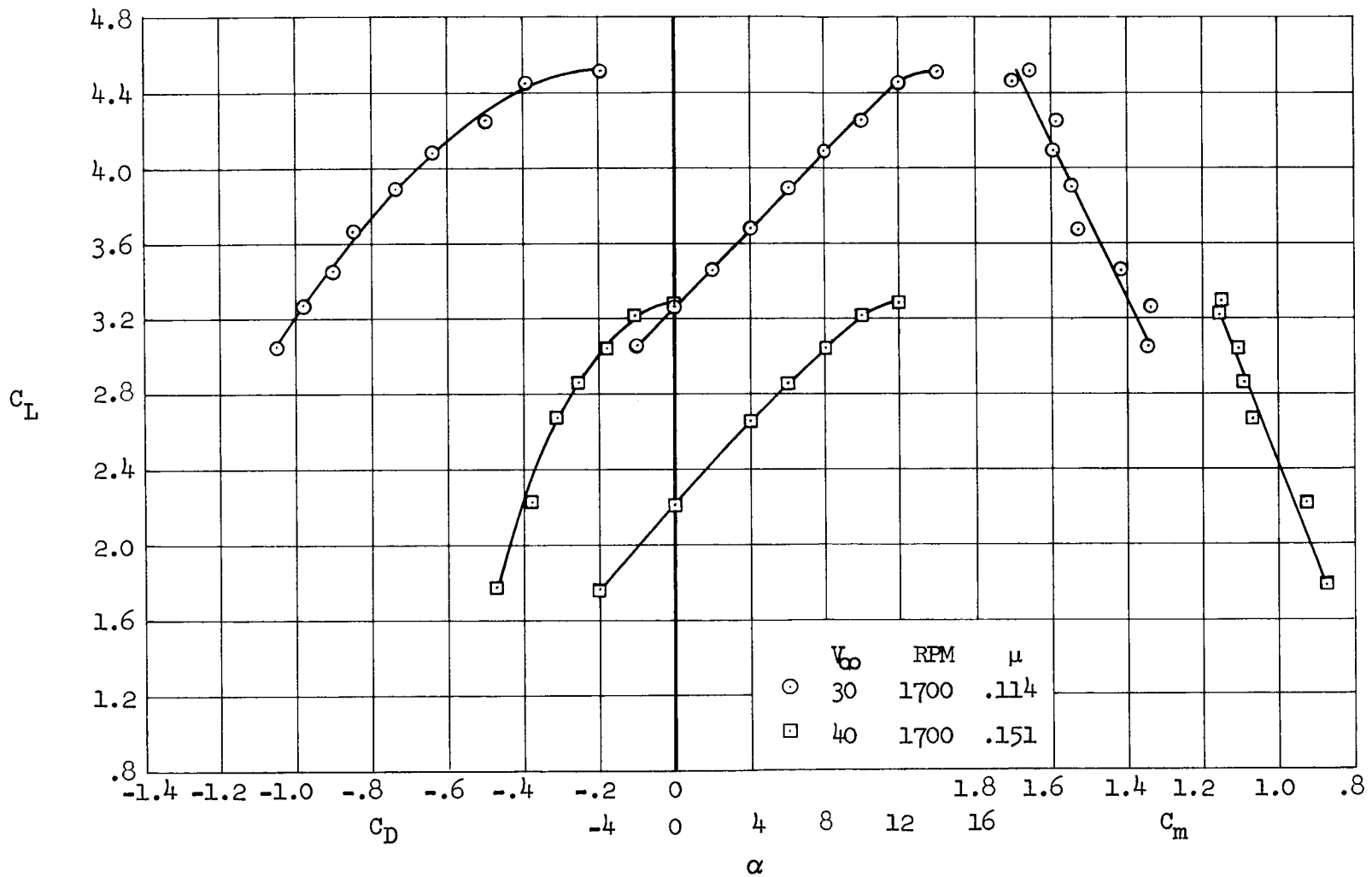

(b) h/d = 2.39

Figure 21.- Concluded

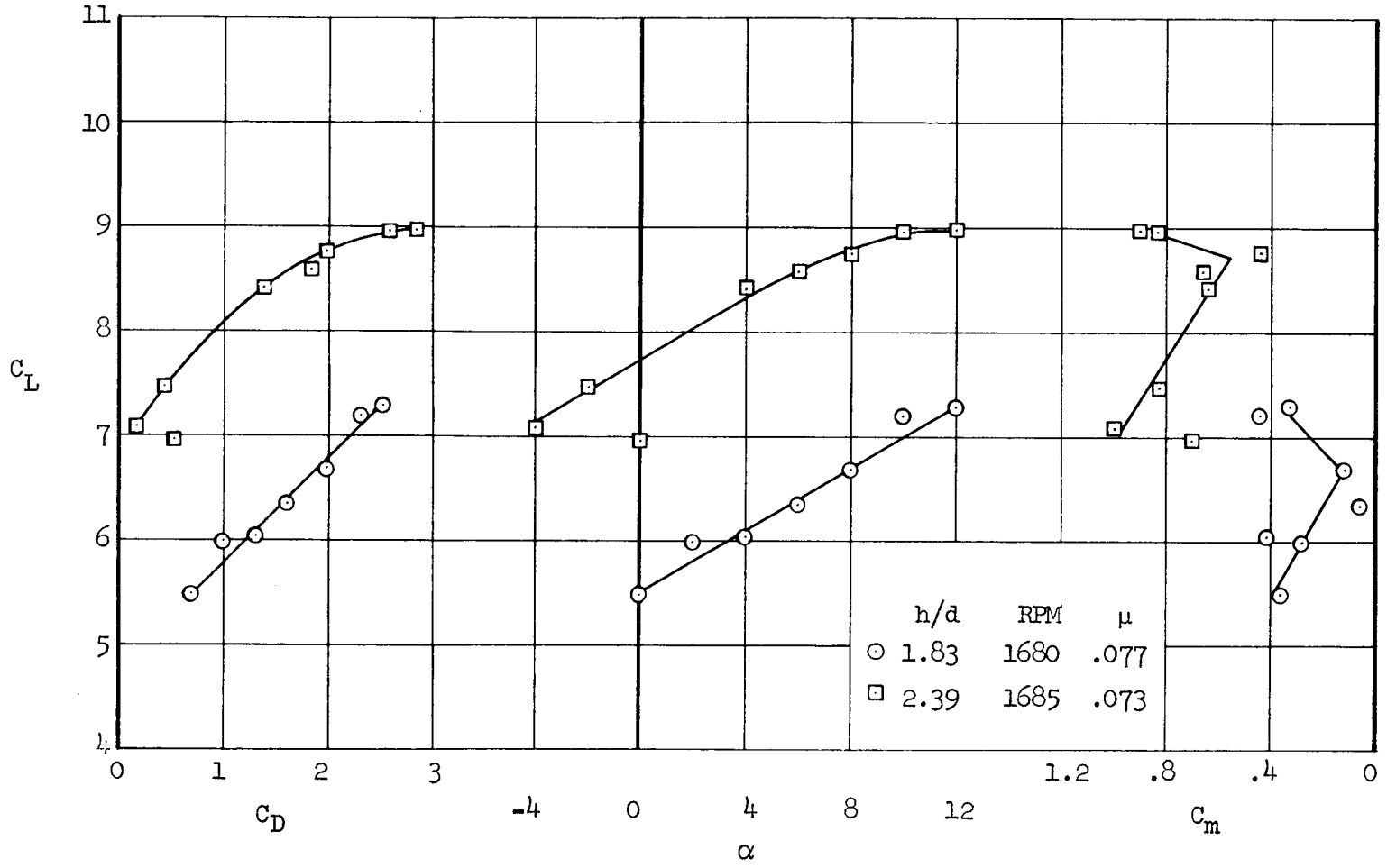

Figure 22.- Power-on longitudinal characteristics; tail on, $\delta_f = 30^\circ$, $\beta = 0^\circ$, $V_\infty = 20$ knots.

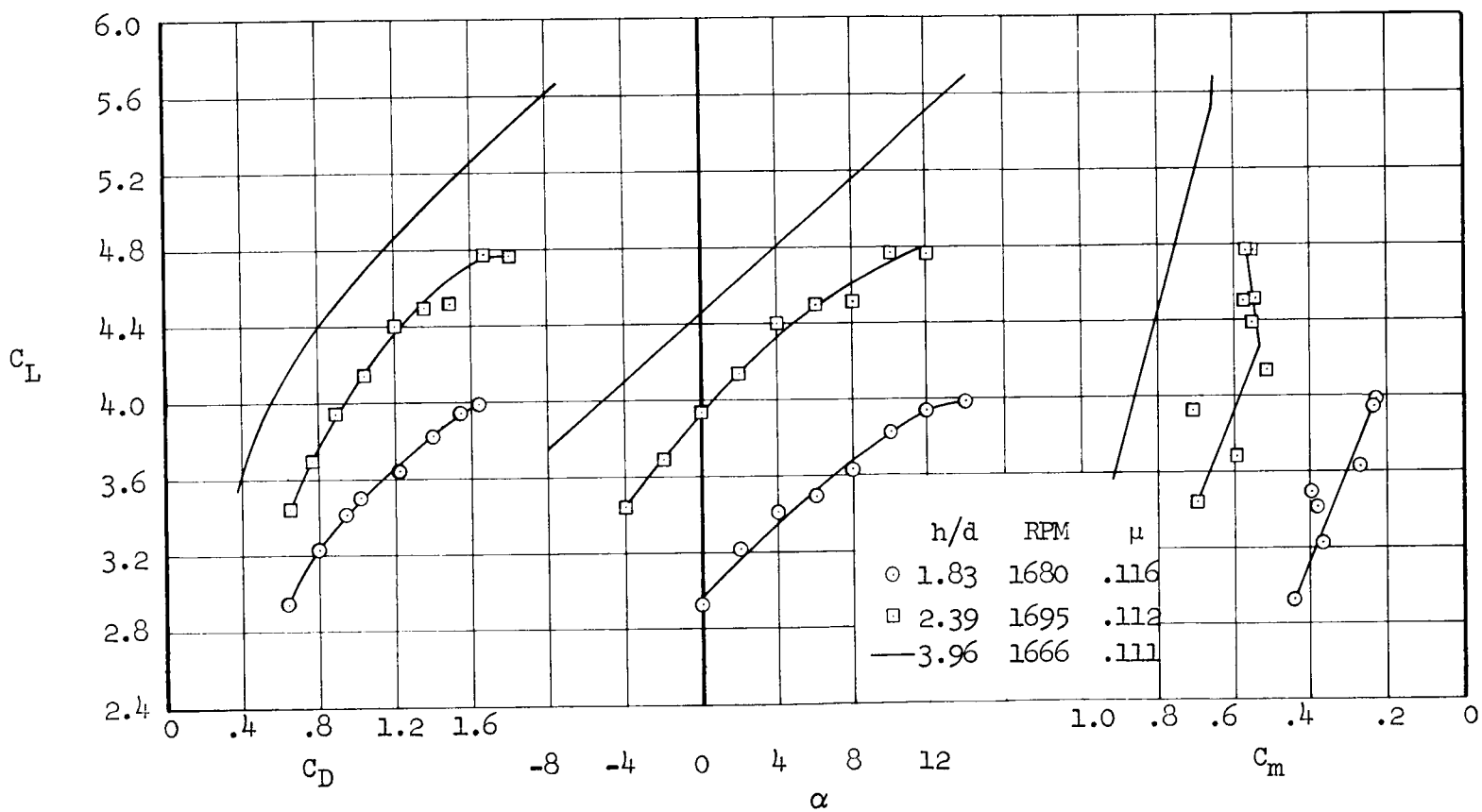

(a) $\beta = 0^\circ$

Figure 23.- Power-on longitudinal characteristics; tail on, $\delta_f = 30^\circ$, $V_\infty = 30$ knots.

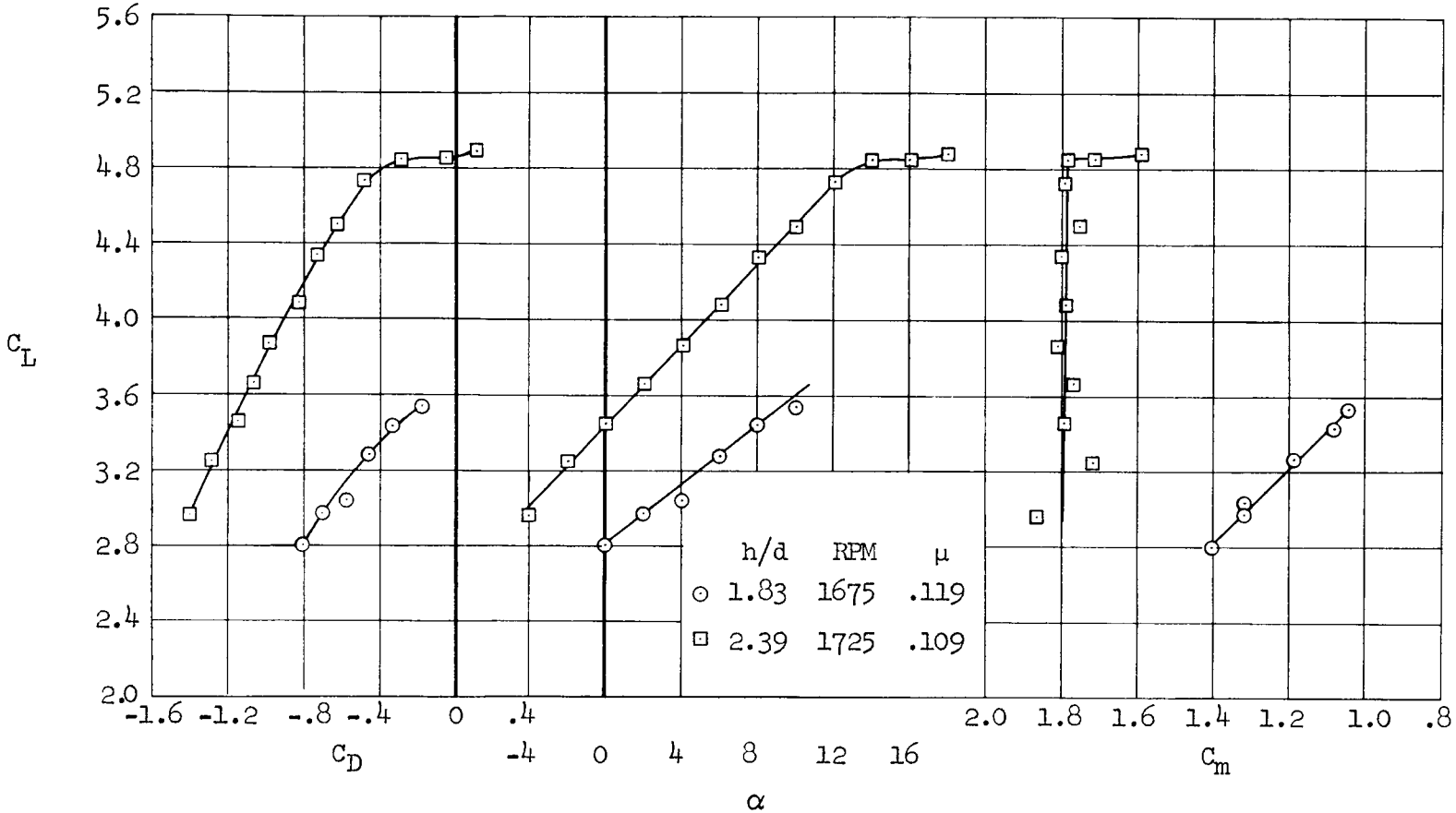

(b) $\beta = 35^\circ$

Figure 23.- Concluded.

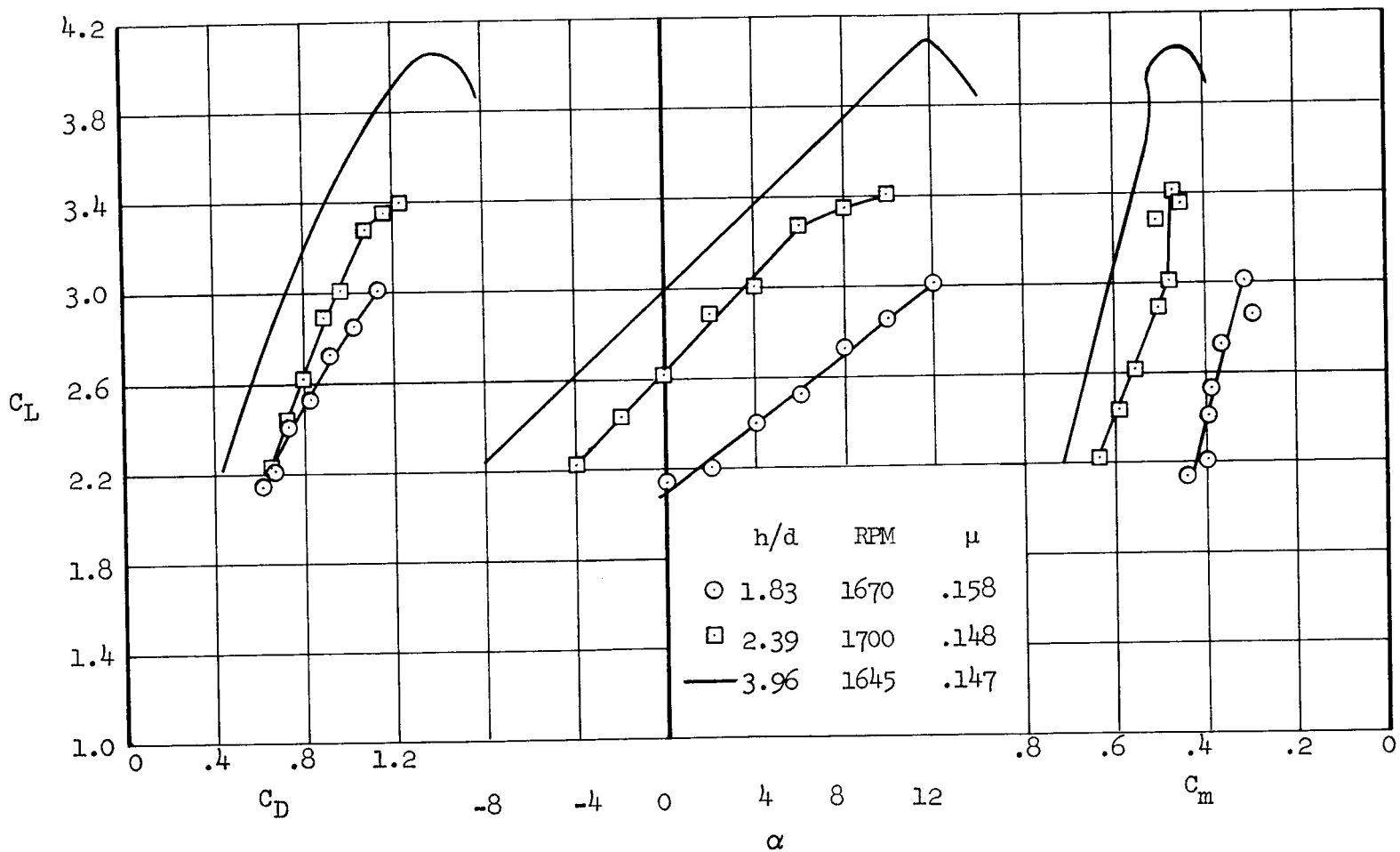

(a) $\beta = 0^\circ$

Figure 24.- Power-on longitudinal characteristics; tail on, $\delta_f = 30^\circ$, $V_\infty = 40$ knots.

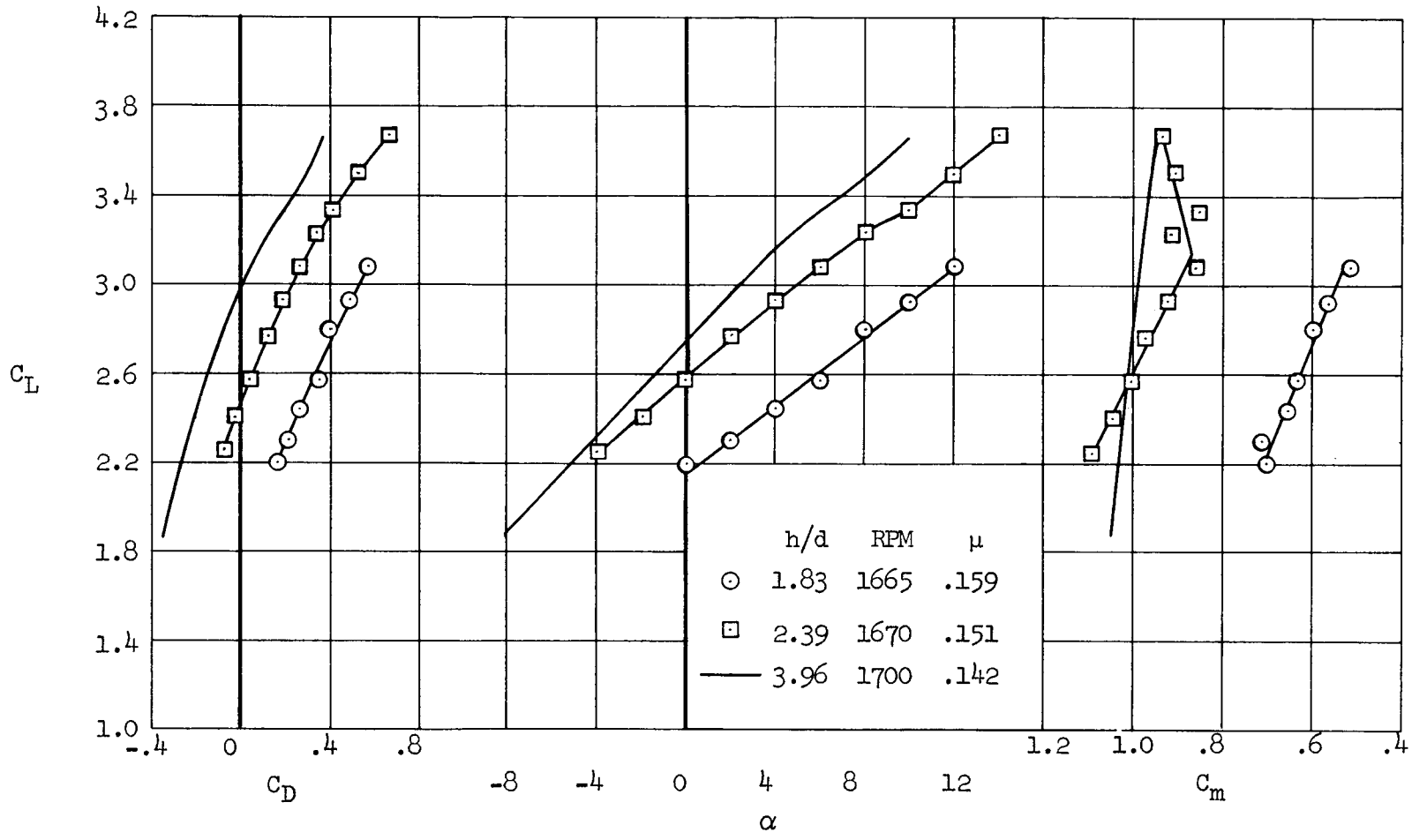

(b) $\beta = 20^\circ$

Figure 24.- Continued.

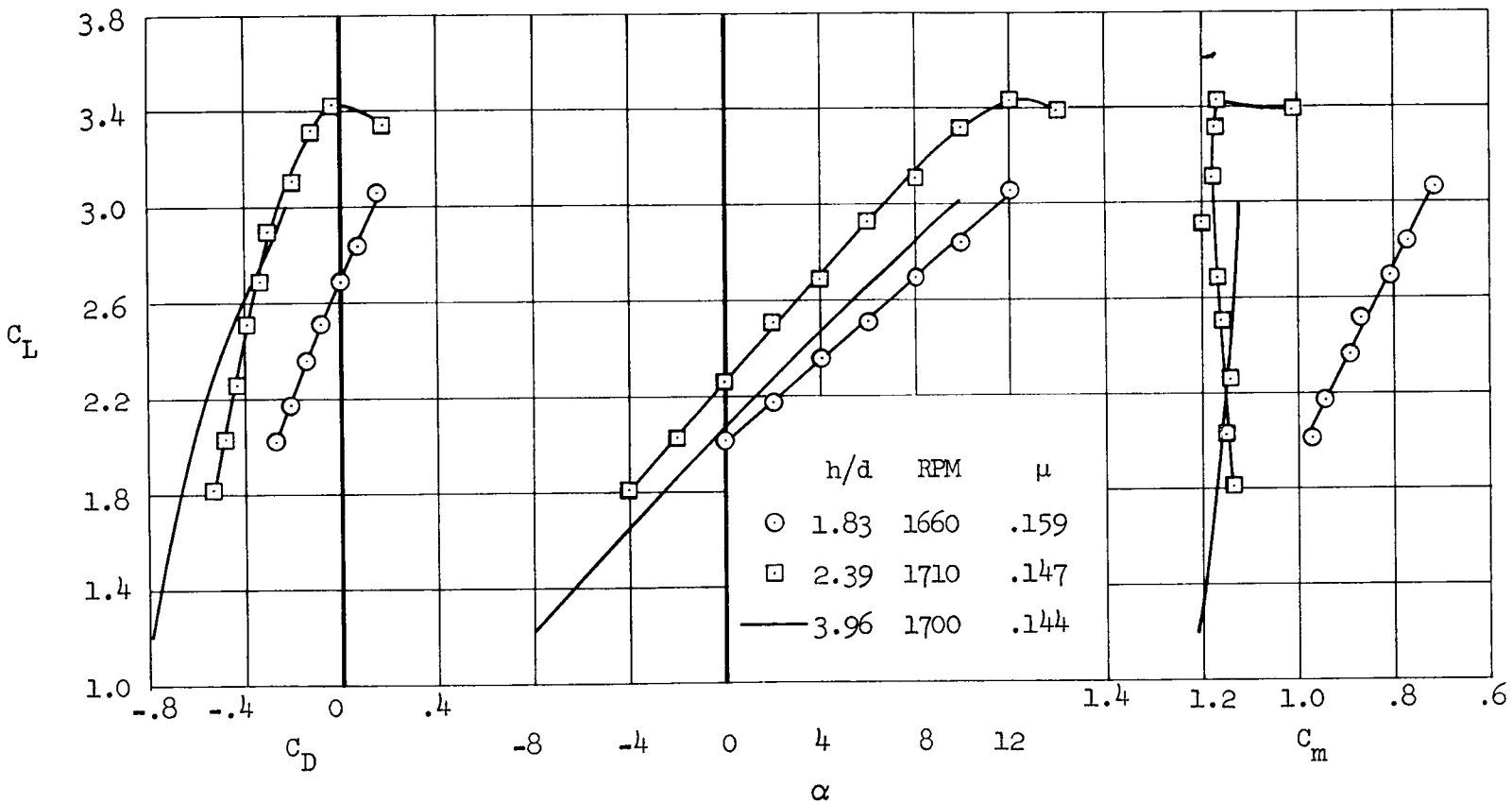

(c) $\beta = 35^\circ$

Figure 24.- Concluded.

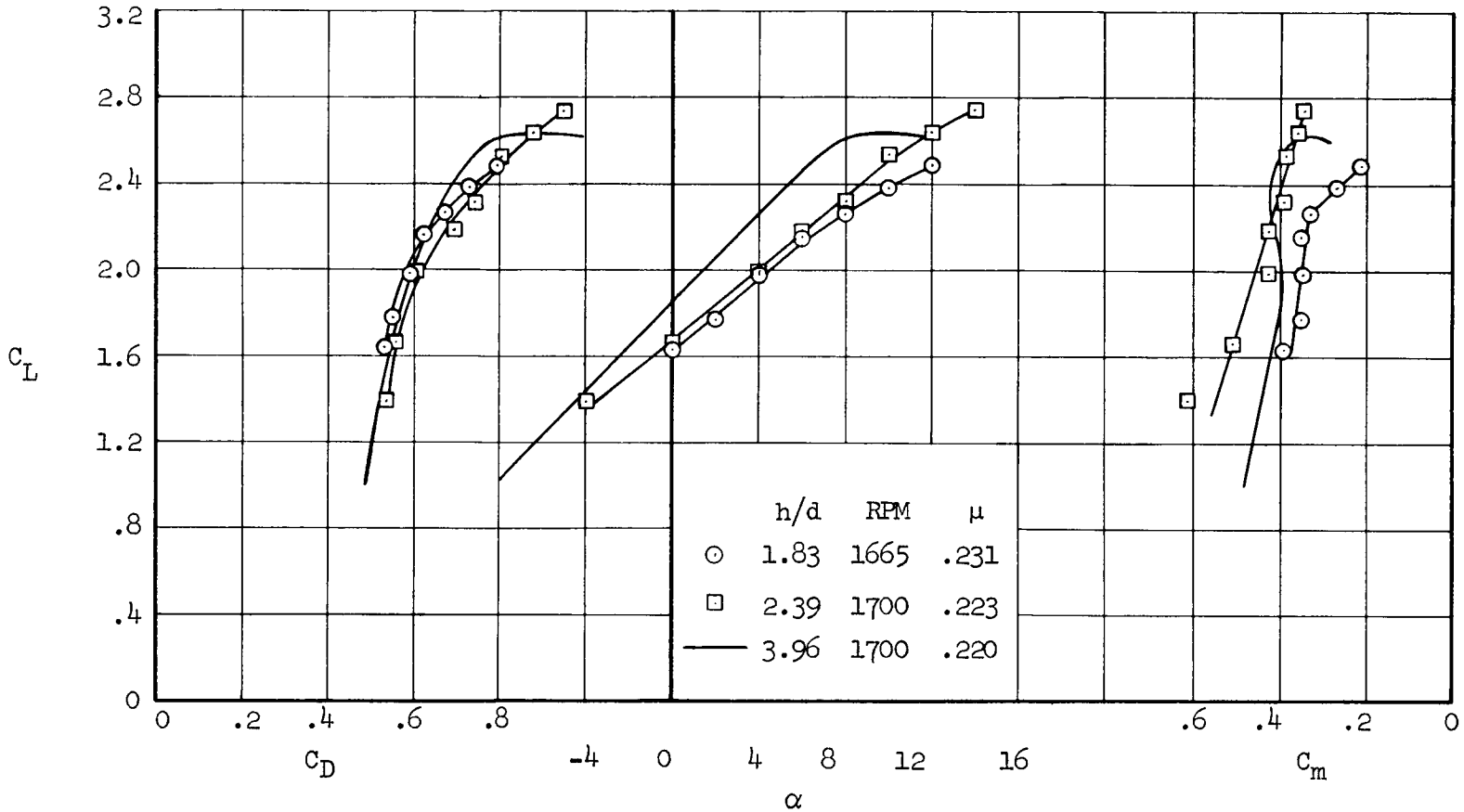

(a) $\beta = 0^\circ$

Figure 25.- Power-on longitudinal characteristics; tail on, $\delta_f = 30^\circ$. $V_\infty = 60$ knots.

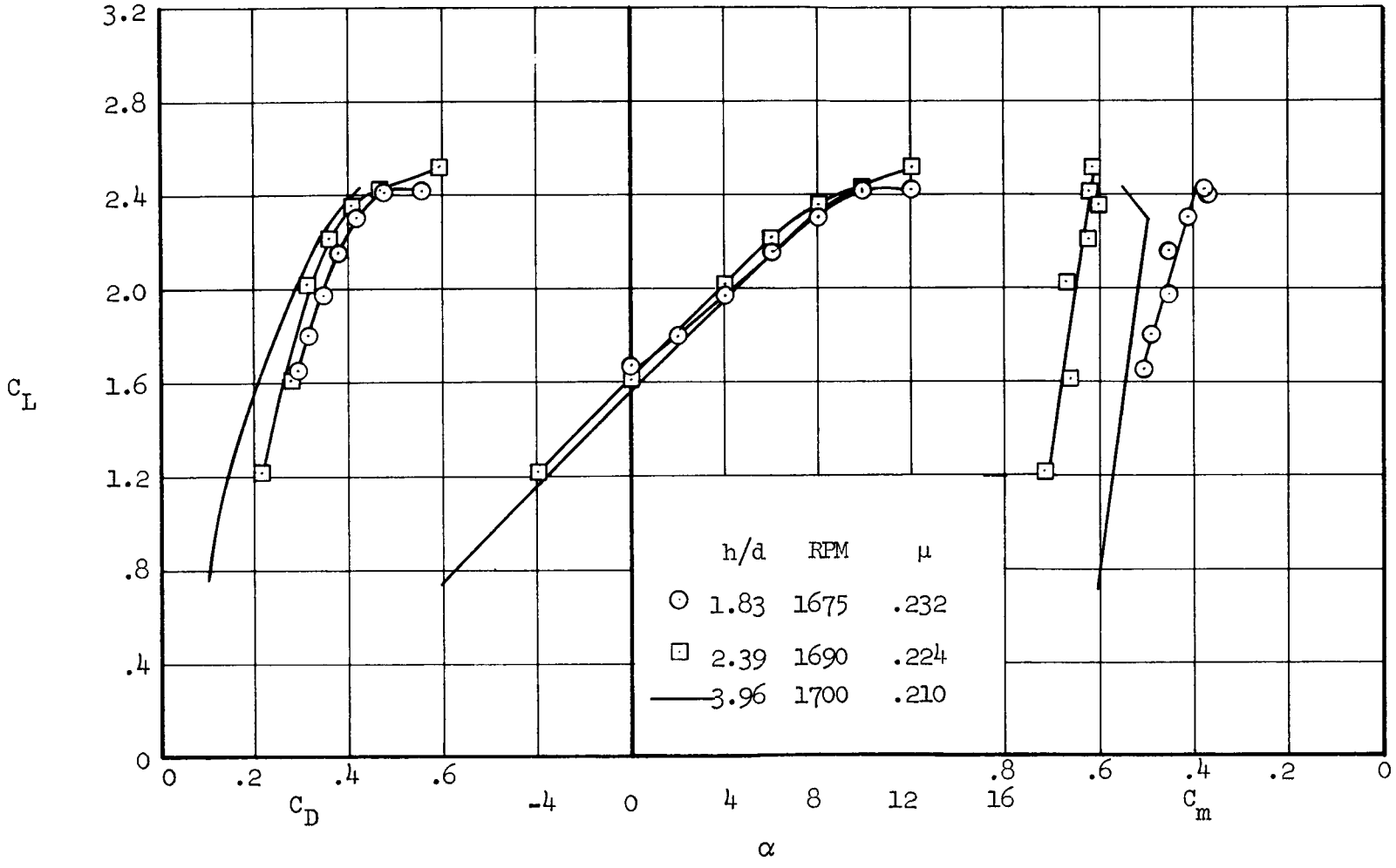

(b) $\beta = 20^{\circ}$

Figure 25.- Continued.

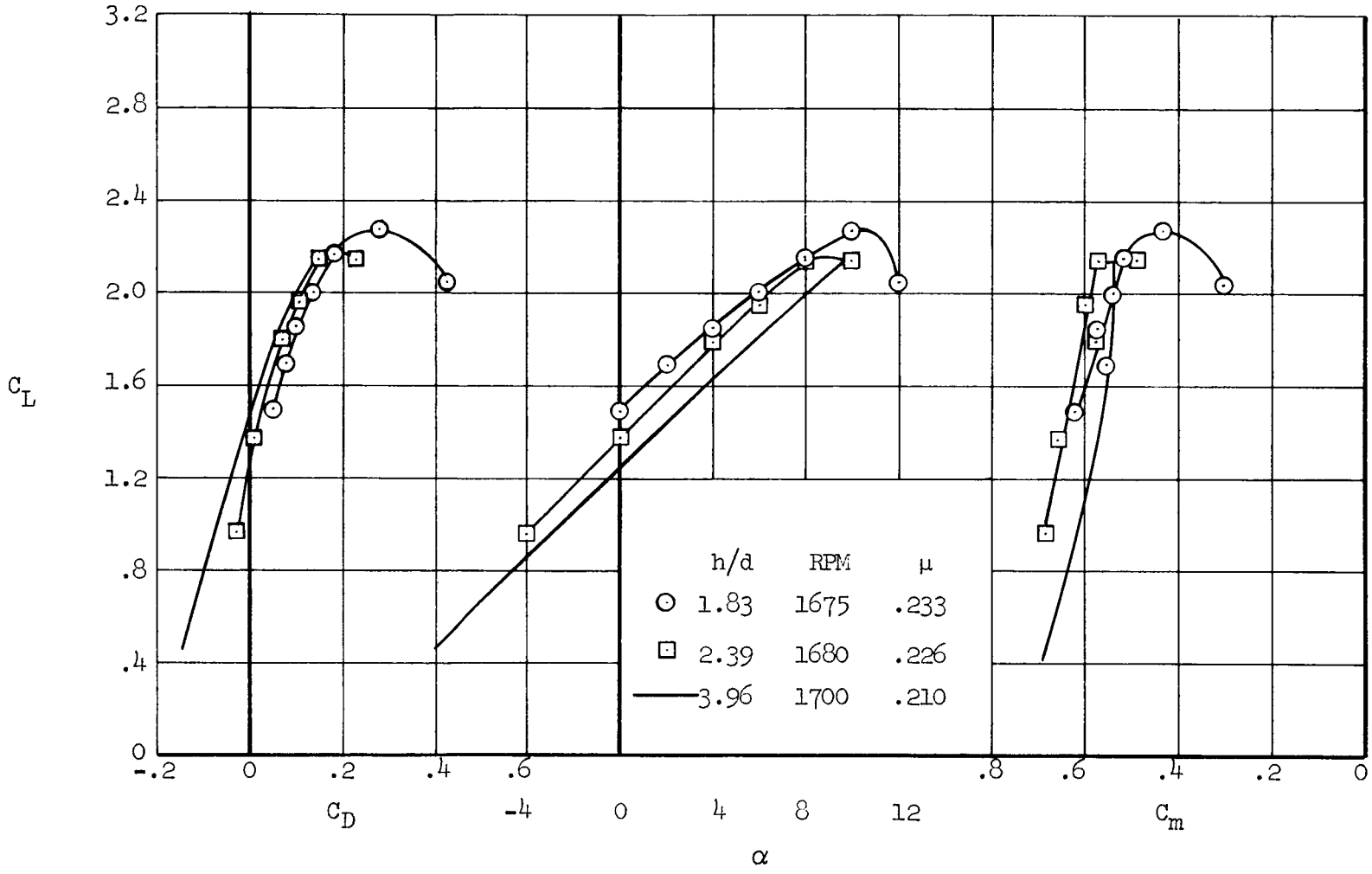

(c) $\beta = 35^{\circ}$

Figure 25.- Concluded.

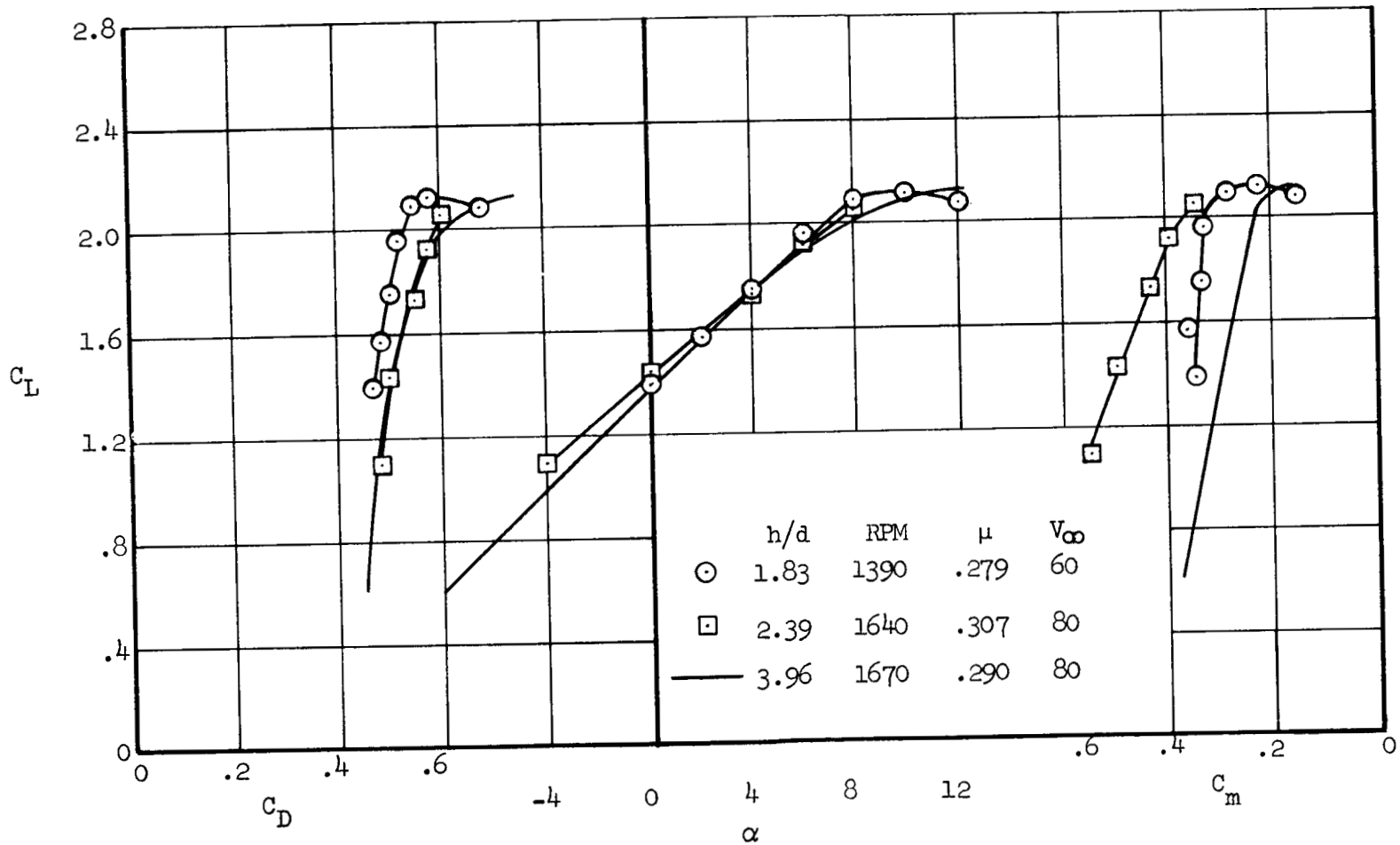

Figure 26.- Power-on longitudinal characteristics; tail on, $\delta_f = 30^\circ$, $\beta = 0^\circ$.

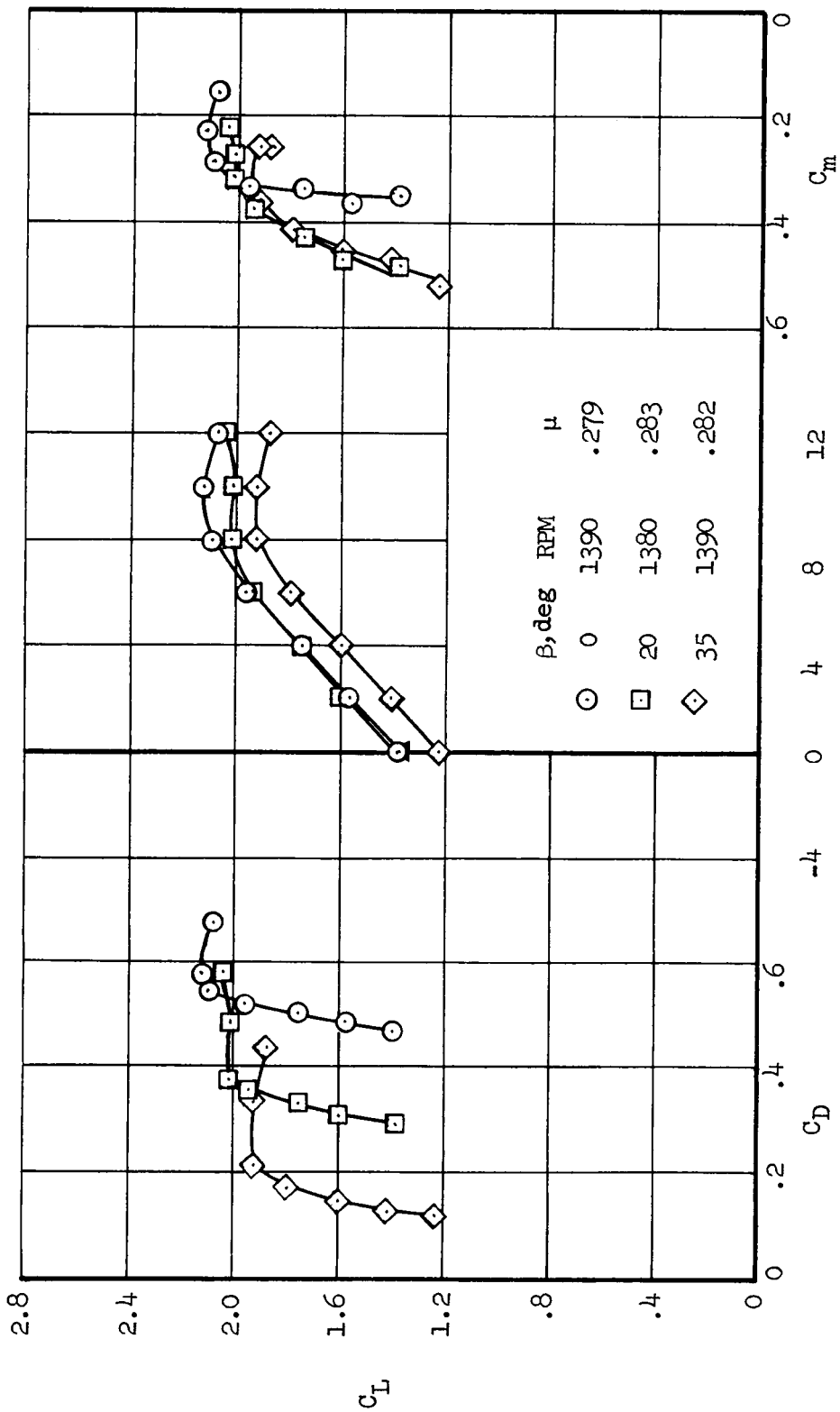

Figure 27.- Power-on longitudinal characteristics; tail on, $\delta_f = 30^\circ$, $V_\infty = 60$ knots, h/d = 1.83.